(4)

Fundamental and Practical Studies of Metal Contacts on Mercury Zinc Telluride

Sponsored by

The Defense Advnced Research Projects Agency (DoD)

Administered through the

The Office of Naval Research

ARPA Order 5674 FRC H414

Contract No. N00014-86-K-0854

Annual Report

January 1, to December 31, 1988

Principal Investigator: W. E. Spicer

Stanford Electronics Laboratories
Stanford University
Stanford, CA 94305-4055
(415) 72304643

Annual Technical Report
DARPA Contract No. N00014-86-K-0854
January 1 - December 31, 1988

A. K. Wahi, G. P. Carey, I. Lindau, and W. E. Spicer
Stanford Electronics Lab, Stanford University, Stanford, CA 94305

Section I - Introduction

Further understanding the role that the weak Hg-Te bond plays during metal/HgCdTe interface formation has been a primary goal of our investigations during this reporting period. Metal/HgCdTe systems in general are highly disruptive, exhibiting a high degree of intermixing of semiconductor substrate components with the overlayer metal. The complexity of the interfaces formed on HgCdTe makes it difficult to isolate the various mechanisms leading to Fermi-level movement in these systems. During this reporting period, we have taken several approaches to investigate these effects under more simplified conditions. We have continued our study of metal/HgCdTe interfaces formed at low temperature, an approach which inhibits metal indiffusion, chemical reaction, and Hg loss, thus leading to a more simplified interface. By lowering the substrate temperature during interface formation, we have been able to observe in more detail the Fermi-level movement which occurs as the overlayer grows. Thus we are able to correlate the observed Fermi-level movement with disruption that occurs as the interface is formed, providing insight into the mechanisms for Fermi-level movement in metal/HgCdTe systems that can also be extended to metal/HgZnTe systems. We have also initiated a study of metal interface formation and Fermi-level pinning for the binary compounds CdTe and ZnTe. Studying the behavior of these related binary semiconductors where the effects of Hg loss are absent gives insight into the role of the weak Hg-bonding in the alloy. Fermi level pinning positions in the binaries are also used to predict and make comparisons between electrical properties of metal contacts to the alloys HgCdTe and HgZnTe, by extrapolation through the range of alloy compositions.

In Section II we describe our effort to reduce the disruption to the HgCdTe surface upon metal overlayer formation over that observed at room temperature by investigating interfaces formed at 100 K between HgCdTe and the three overlayer metals Ag, Al, and Pd. The metals were deposited onto the [110] cleaved HgCdTe surfaces in UHV in increments ranging from submonolayer at low coverages to tens of monolayers at high coverages, and the formation of the interfaces were monitored using photoemission spectroscopy subsequent to each deposition. The primary experimental observation of this study is that deposition of all three of these metals onto HgCdTe substrates held at reduced temperatures causes the surface Fermi level (E_f) to move from its initial, as-cleaved position, typically located at or near the conduction band minimum, into the conduction band, and this movement is correlated with the absence of the movement of the overlayer metal into the semiconductor. This phenomenon is observed at the lowest coverages (submonolayer) for all three overlayer metals, and for the case of Ag grown at 100 K, is observed for higher coverages as well. The final positions of E_f for the three overlayer growths match very closely to those seen for the corresponding room temperature growths.

Section III presents our investigation of interfacial morphology and Fermi level pinning behavior at the interfaces of Al, Ag, and Pt with UHV-cleaved CdTe and ZnTe. Results are compared to metal/HgCdTe interface formation, where the weak Hg-Te bond and consequent ease of Hg loss strongly influence semiconductor disruption and metal-semiconductor intermixing. For Al/CdTe, we observe a case where the strong Al-Te reaction yields a significantly more extensive Al-Te reacted region than has been observed for HgCdTe. The Al/ZnTe interface is observed to be more abrupt than Al/CdTe. The final Fermi level pinning positions $E_{fi} = E_f - E_{vbm}$ for Al, Ag, and Pt on p-type CdTe and p-ZnTe have been determined. E_{fi} is found to be roughly the same for both CdTe and ZnTe, with the value for ZnTe lying approximately 0.2 eV closer to the VBM for all three metals. From these results, one would expect Schottky barriers of about the same height for these metals on p-CdTe and p-ZnTe; and also that, in principle, metal interfaces with the two alloys

HgCdTe and HgZnTe would have the same electrical properties. Comparisons and implications for electrical behavior of metal contacts to the alloys are discussed.

The interface formed in UHV between the HgCdTe substrate held at RT and Pd is among the most complex observed at metal/HgCdTe interfaces. Section IV describes the experimental evidence for Hg, Cd, and Te dissociation from the HgCdTe substrate during the initial stages of formation of the Pd/HgCdTe (x = 0.39) contact in UHV. The dissociation of all substrate constituents from the substrate and their subsequent intermixing into the overlayer metal has not been observed for any other metal/HgCdTe interfaces reported to date. The heats of alloying between the overlayer metal Pd and the substrate cations are shown to play a dominant role in the interface chemistry. The bulk thermodynamic data between Pd and the HgCdTe constituents indicates that Pd will chemically interact with not only Te from the substrate, but with the cations Cd and Hg as well. Experimental observations at the interface between Pd and CdTe are then presented, in which the difference in interface morphology between the Pd/CdTe and Pd/HgCdTe interfaces is correlated to the presence of the weak Hg-Te bond in the HgCdTe lattice.

Section II - Fermi Level Movement at Metal/HgCdTe Contacts Formed at Low Temperature

I. INTRODUCTION

Gaining insight into the mechanisms that induce surface Fermi level (E_f) movement at metal/HgCdTe interfaces is rendered difficult since the formation of metallic contacts at room temperature (RT) on HgCdTe typically disrupts the HgCdTe lattice, leading to a complicated interface exhibiting Hg loss from the substrate and intermixing between the metal and the substrate constituents.[1,2] Theoretical models[3,4,5] examined by Spicer [6] follow the predicted movement of the surface Fermi level at the metal/semiconductor interface when going from the binary to the alloy. For the case of $Hg_{1-x}Cd_xTe$ system, the pinning of the Fermi level position for metals on the binary CdTe[7-11] has been studied more extensively than for the alloy and is perhaps better understood since interfaces formed on CdTe tend to be more abrupt with a less complicated morphology than for HgCdTe. All three of the theoretical models discussed by Spicer[6], the metal induced gap states (MIGS)[3], the effective work function model[4], and the defect model[5], predict that ohmic contacts (rectifying contacts) are to be expected for metal overlayers on *n*-type (*p*-type) HgCdTe of *x*-value lower than approximately 0.4 to 0.5. In order to better isolate the mechanisms behind the Fermi level movement at metal/HgCdTe ($x < 0.5$) interfaces, and consequently gain better insight into the appropriate mechanisms leading to the Fermi level pinning position at these interfaces, a simplification of the physical interface is necessary. A successful effort to reduce these effects by lowering the substrate temperature during metal overlayer growth has been reported[12] that shows a decrease in Hg loss and reduction of intermixing for the Ag/HgCdTe and Al/HgCdTe interfaces formed at 170 K.

In an effort to further reduce semiconductor disruption during metal deposition over that seen for the corresponding room temperature interfaces, we employ in this study a lower HgCdTe substrate temperature (100 K) during the overlayer growth of the three metals Ag, Al, and Pd. These three metals exhibit vastly different heats of formation with Te at room temperature

($\Delta H_f(Ag_2Te)$ = -8.6 kcal/mol[13], $\Delta H_f(Al_2Te_3)$ = -76.2 kcal/mol[13], and $\Delta H_f(PdTe)$ = -9 kcal/mol[14]). Heats of solution between the metal and the substrate cations should also be considered if the values are comparable or greater than the metal/anion heats of formation[15,16], and calculations based on the semiempirical model of Miedema *et al.*[17] give the heats of solution between the cations and Pd as: ΔH_{sol}(Cd:Pd) = -32.4 kcal/mol and ΔH_{sol}(Hg:Pd) = -26.2 kcal/mol. The room temperature UHV interfaces between HgCdTe and Ag[18,19], Al[18,20,21], and Pd[22] overlayers have been studied previously and exhibit vastly different interface morphologies. These three metals also give different doping characteristics in bulk HgCdTe, where Ag (*n*-type), Al (*p*-type), and Pd (unknown), and the systematics of the RT band bending observed for Ag and Al overlayers as well as other metal/HgCdTe systems suggest that the final Fermi level pinning position at these interfaces is largely influenced by the doping of the HgCdTe by the overlayer metal.[2] By lowering the substrate temperature during the formation of these overlayers onto HgCdTe, the possible mechanisms of Fermi level movement in the absence of interdiffusion and intermixing of the overlayer metal and the HgCdTe substrate can be investigated.

II. EXPERIMENTAL

Bulk *p*-type HgCdTe single crystals of cross section 5 x 5 mm were introduced into a previously baked ultra-high vacuum (UHV) chamber ($p < 10^{-10}$ Torr). The crystals were grown at Santa Barbara Research Center. The samples were cooled to 100 K by placing them in thermal contact with a liquid-nitrogen reservoir, where the temperature of the sample was monitored via a thermocouple attached to the foot of the sample holder. Upon reaching 100 K, the crystals were cleaved in UHV to reveal an atomically clean (110) face. The surfaces converted to *n*-type upon cleaving, which is commonly observed for cleaved HgCdTe.[23] The metals were deposited onto this surface from previously out-gassed W filaments in increments ranging from sub-monolayer at low coverages to several monolayers at higher coverages. A quartz-crystal microbalance was placed next to the sample surface to monitor the metal flux to the surface. The surfaces were monitored after each deposition with the surface sensitive technique of photoemission spectroscopy

(PES) using tunable synchrotron radiation, Mg Kα (1253.6 eV), and the He I (21.2 eV) and He II (40.8 eV) emission lines from a He resonance lamp. Each interface was formed with $Hg_{1-x}Cd_xTe$ of different x-value: Ag on x = 0.23, Al on x = 0.30, and Pd on x = 0.39. The Ag/HgCdTe interface was studied using synchrotron radiation dispersed with a grasshopper monochromator, giving accessible energies between 65 and 200 eV. The Al, and Pd were monitored with the conventional laboratory sources, which enabled a more bulk probing (escape depth λ of the electrons in the range of 10-20 Å) than for the Ag study (λ ≈ 5 Å). The photoelectrons were analyzed using a double pass cylindrical mirror analyzer with an integrating acceptance angle of 42.3 ± 3°. The amount of each metal deposited is given in monolayers (ML), which we define as the surface density of atoms at the (110) surface of HgCdTe: 1 ML = 6.8 x 10^{14} atoms/cm^2, which corresponds to 1.15 Å of metallic Ag, 1.12 Å of metallic Al, and 0.99 Å of metallic Pd.

III. RESULTS

Results obtained in this study are described in the next three sections. The description of the movement of the bands and the E_f are used interchangeably since the valance band maximum (VBM), conduction band maximum (CBM), and the core levels are all tied to the same energy reference, an identical movement of the core level centroids indicates an equal movement of the VBM and CBM. Hence, movement of the core levels to deeper BE indicates a downward movement of the VBM with respect to the E_f, which is also visualized as an upward movement of the E_f away from the VBM. The BE of the Hg 5d relative to the VBM of the $Hg_{1-x}Cd_xTe$ alloy system has been experimentally determined using angle-resolved photoemission spectroscopy.[24,25] From the BE value of -7.95 ± 0.1 eV for Hg $5d_{5/2}$ in HgTe [24], the decrease in the BE with x-value is given by

$$BE = E(Hg\ 5d_{5/2};Hg_{1-x}Cd_xTe) - E(VBM) = E(Hg\ 5d_{5/2};HgTe) + 0.35x,$$

taken from Ref. [25]. Thus, for the x-values employed in this investigation, the BE of the Hg $5d_{5/2}$ core level is taken as: 7.85 ± 0.1 eV (for x = 0.23 and 0.30), and 7.80 ± 0.1 eV (for x =

0.39). In placing the E_f with respect to the CBM, the bandgap of HgCdTe is taken from Ref. [26], which at 100 K is: 0.14 eV (for x = 0.23), 0.25 eV (for x = 0.30), and 0.39 eV (for x = 0.39).

A. Ag/HgCdTe

PES spectra of the Hg 5d, Cd 4d and Ag 4d core levels showing the movement of the bands of HgCdTe (x = 0.23) upon Ag contact formation and annealing are shown in Fig. 1, where the BE is referenced to E_f. The spectra were taken at 80 eV photon energy to provide maximum surface sensitivity (2-3 atomic layers). The top spectra is taken from the cleaved surface, where the BE of the Hg $5d_{5/2}$ core level relative to the E_f is found to be 8.12 ± 0.05 eV. Since the VBM is located 7.85 ± 0.1 eV above this core level centroid, this places the E_f at 0.27 eV ± 0.1 eV above the VBM. Therefore the surface has converted to *n*-type upon cleaving. Also shown are the core level spectra taken at 54 ML coverage at 100 K and after annealing at RT for one hour. This was the highest coverage studied, and the bands are located 0.2 eV to deeper BE before the RT anneal, placing the E_f at 0.57 ± 0.1 eV above the VBM. After the 1 hour RT anneal, the bands move back close to the original position seen at the cleaved surface, indicating that the E_f moves back toward the VBM. The Ag 4d intensity decreases after the anneal and Hg 5d and Cd 4d intensity increases slightly, indicating that the Ag could be diffusing into the substrate.

The ability to obtain spectra from the substrate core levels at this high coverage indicates that the Ag could be islanding even for this low temperature growth. There is a slight decrease in the Hg 5d signal with respect to the Cd 4d, therefore for the highest coverage there is discernable Hg loss from the top 2-3 atomic layers of the surface, although it is slight. For the Ag/HgCdTe interface formed at 170 K[12], a laminar overlayer growth of Ag was observed, but it this does not occur for this 100 K growth. However, the Ag 4d signal increases monotonically with deposition, indicating that Ag is building up on the surface. This was not observed at the RT Ag/HgCdTe interface[18,19], where for similar coverages very little Ag signal was detected which was interpreted as Ag diffusing into the bulk 1000's of Å. Since islanding of Ag should be diminished at this

lower temperature, it is possible that the cleavage quality could lead to the difference in the interface morphology.

B. Al/HgCdTe

The Hg 5d and Cd 4d shallow core levels arising from the HgCdTe (x = 0.30) substrate taken as a function of Al overlayer coverage are shown in Fig. 2, where the BE is referenced to E_f. The spectra are taken with hν = 21.2 eV, hence the signal arises from the top 15 to 20 Å of the surface. At the cleave, the Hg $5d_{5/2}$ core level is located at 8.35 ± 0.05 eV BE with respect to the E_f, placing the E_f 0.5 eV above the VBM. Thus the cleaving process inverted the surface to *n*-type. Even at the lowest coverage of Al (0.1 ML), the bands move to deeper BE and remain at this position for all subsequent coverages. The movement of the bands to 0.12 eV deeper BE upon metal deposition indicates that the E_f moves to 0.62 ± 0.1 eV above the VBM, and with subsequent Al metal depositions remains near this value. At 0.7 ML coverage, the Hg 5d signal has decreased much more than the Cd 4d signal, indicating Hg loss from the substrate surface even at these lowest coverages. Only the submonolayer coverages are shown since no additional band bending occurs at the higher coverages.

C. Pd/HgCdTe

Fig. 3 shows the Hg 5d and Cd 4d shallow core levels arising from the HgCdTe (x = 0.39) surface as a function of Pd overlayer coverage Θ in ML, where the BE is referenced to the E_f. The spectra were taken with He I (hν = 21.2 eV), hence arise from the top 15 to 20 Å of the surface. The position of the Hg $5d_{5/2}$ core level is 8.23 ± 0.05 eV below the E_f at the cleave, placing the E_f 0.43 ± 0.1 eV above the VBM at the cleave surface. Thus the E_f position is near the CBM for this cleaved surface. The bands bend to deeper BE reference to the E_f at the lowest coverage (0.3 ML) and move back slightly towards the cleave position with increasing coverage. At 0.3 ML coverage, the Hg $5d_{5/2}$ centroid is located at 8.40 ± 0.05 eV, which places the E_f at 0.6 ± 0.1 eV above the VBM for this low coverage. At 3 ML coverage, a slight shoulder to the lower BE side

of both the Hg 5d and CdTe appears and at higher coverages dominates the signal from both cores. These peaks are associated with dissociated Hg and alloyed Cd[22], indicating that chemistry and surface disruption occurs as more Pd is deposited. The substrate peaks shift to 0.1 eV lower BE at the intermediate coverages, indicating a E_f movement back to 0.5 ± 0.1 eV above the VBM. Also shown is a spectra at 42 ML coverage taken after annealing the surface at RT for 48 hours. The Hg 5d and Cd 4d signals arising from dissociated Hg and alloyed Cd both increase but little or no signal is observed from the HgCdTe substrate. This suggests that little or no intermixing between the reacted overlayer and the HgCdTe substrate occurs on an atomic scale for this thin Pd on HgCdTe contact.

IV. DISCUSSION

For each metal/HgCdTe overlayer investigated in this study, the initial movement of the E_f is from its cleaved position, near the CBM, to higher into the conduction band (CB). At higher coverages for the Al and Pd case and upon annealing for the Ag case, the E_f moves to a final position consistent with that observed at similar interfaces formed at RT. The position of E_f above the VBM is shown schematically for each case in Fig. 4. Plotted in this figure are: the position of E_f at the cleave, the maximum position of E_f above the VBM, and the final position of E_f for each metal/HgCdTe interface studied. All of the E_f-VBM values have an error bar of ± 0.1 eV, to which the largest contribution is due to the inaccuracy in knowing the exact position of the VBM.[24,25]

The initial movement of the E_f higher into the CB to a position of 0.6 ± 0.1 eV observed at these interfaces is not seen at the RT grown Ag[18,19] interface. For this case, the E_f moves very little: 0.05 eV below the cleaved position for the RT Ag grown interface. The RT Ag/HgCdTe interface is known to be diffuse, with the Ag diffusing deep into the HgCdTe, whereas the lower temperature (LT) interface between Ag and HgCdTe is much more abrupt. The PES data shown here as well as the PES data taken from the 170 K grown interface[12] reveal that there much less diffusion of Ag into the substrate at these lower growth temperatures. In the absence of the Ag

diffusing into the lattice, the E_f is observed to move upward. The annealing of the interface at RT for 1 hour is sufficient for the Ag to move into the lattice and hence become an acceptor impurity in the HgCdTe. The downward movement of the E_f upon annealing is consistent with the Ag, a known *p*-type dopant in bulk HgCdTe, doping the lattice. Although the E_f moves downward in this case, it does not move far enough toward the VBM to render the surface *p*-type. This is perhaps due to the E_f being pinned near or above the CBM at the cleaved surface, and the electrically active damage introduced to the lattice upon cleaving cannot be fully compensated. Nevertheless, the E_f is observed to move quite a distance even with such damage.

The upward movement of the E_f high into the CB for the Pd/HgCdTe interface studied here is not observed at the RT interface[22], where the movement of the E_f is negligible. In both cases, dissociation of the cations from the lattice occurs, causing the interface to be highly disrupted. However, for the case studied here, the dissociation of the cations occurs at higher coverages than for the RT interface. For the case studied here at low coverages (< 3 ML), there is no detecable intermixing and an abrupt interface is evident. The maximum position of the E_f above the VBM corresponds to this "ideal" interface. When the disruption begins to be evident, the E_f moves downward 0.1 eV. Pd has unknown doping characteristics in bulk HgCdTe, but this data is suggestive of Pd having acceptor-like behavior in HgCdTe. The chemistry and dissociation of the cations at the Pd/HgCdTe interface is discussed in much detail in Ref. [22].

For the Al/HgCdTe interface formed at 100 K, a similar movement to that observed for the RT interface[18,20,21] is seen, where the E_f moves high into the CB. Since one cannot distinguish the movement of the E_f between the two growth cases, it is difficult to attach significance to the initial upward movement of the E_f for the LT case. However, the LT interface exhibits much less Hg loss than the corresponding RT interface, and at low coverages, the damage to the underlying HgCdTe lattice is reduced. Morphologically, the interface appears "ideal" at the lowest coverages of Al, but beginning with the 0.7 ML coverage of Al some Hg loss from the lattice is observed. The movement of the E_f at the undisrupted interface is the same as that seen for the Ag and Pd

grown on HgCdTe at LT. At the higher coverages, where Hg loss and reacted Te are evident, the interface becomes much more complex, and the lack of movement of the E_f at this LT interface is consistent with the Al, an *n*-type donor in bulk HgCdTe, doping the lattice.

Since Ag and Al are known to be *p*- and *n*-type, respectively, dopants in bulk HgCdTe, and the Pd doping behavior is unknown, these observations are consistent with the metal atoms, prior to their diffusing into the substrate or chemically reacting with the substrate atoms, donating electronic charge to the semiconductor, hence raising E_f into the CB. When the interface becomes disrupted upon warming or increased deposition, the metal atom can diffuse into the semiconductor, doping the lattice. Fig. 5 shows surface band diagrams for the three stages of LT interface formation on HgCdTe. For simplification, the diagrams are drawn for the very near surface, so band bending is not shown. From the position at the cleave, the E_f moves higher into the CB for all three systems at the ideal interface, rendering the surface degenerate *n*-type. Upon forming a disrupted interface, the E_f moves in the direction consistent with the doping of the lattice by the overlayer metal. The electronegativities (EN) for the three metals are shown in the diagram, where Pd (2.2) and Ag (1.9) are observed to have relatively high values of EN. It appears that ohmic (rectifying) contacts are to be expected on *n*-type (*p*-type) HgCdTe ($x < 0.4$ to 0.5) even for metals of high EN (workfunction) if the HgCdTe is not disrupted. Hence, reducing the disruption to the HgCdTe lattice upon contact formation will probably not achieve ohmic contacts to *p*-type HgCdTe, and that the introduction of suitable *p*-type dopants during metal contact formation is probably necessary to accomplish this task.

V. CONCLUSIONS

The Ag, Al, and Pd metal/HgCdTe interfaces formed on the (110) surface held at 100 K during growth exhibit similar band bending behavior for the undisrupted interfaces, where the E_f is observed to move from the initial position observed at the cleaved surface to 0.6 ± 0.1 eV above the VBM, which places it high into the CB for the *x*-values studied. Upon disruption to each interface, the E_f moves toward the position observed for the corresponding RT interface. For the

Ag/HgCdTe, the movement of the E_f back toward the VBM occurs after annealing the interface at RT for 1 hour, which is consistent with Ag, a *p*-type dopant in bulk HgCdTe, diffusing into the substrate and doping the lattice. For the Al/HgCdTe case, the E_f remains high into the CB upon disruption of the interface caused by increased deposition of Al, consistent with Al, a *n*-type dopant in HgCdTe, doping the lattice. The E_f at the Pd/HgCdTe interface moves slightly toward the VBM upon disruption caused by increased deposition of Pd onto the HgCdTe surface held at 100 K. Both Ag and Pd have high EN (workfunction), hence the upward movement of E_f into the CB is seen even for metal overlayers of high EN. These observations suggest that intrinsic ohmic (rectifying) contacts are to be expected on *n*-type (*p*-type) HgCdTe (for *x*-value < 0.4 to 0.5) even for interfaces that undergo little or no disruption during contact formation, and that the movement of the E_f into the bandgap may only be possible by doping the surface during contact formation by suitable *p*-type dopants.

ACKNOWLEDGEMENTS

*Work funded by DARPA under contract # N00014-86-K-0854.

REFERENCES

a) Stanford Ascherman Professor of Engineering.

1 G. D. Davis, Vouto **16**, 127 (1986), and references therein.

2 D. J. Friedman, G. P. Carey, I. Lindau, and W. E. Spicer, J. Vac. Sci. Technol. A **5** 3190 (1987) , and references therein.

3 J. Tersoff, Phys. Rev. B **32**, 6968 (1985).

4 J. L. Freeouf, and J. M. Woodall, Appl. Phys. Lett. **39**, 727 (1981).

5 W. E. Spicer, P. W. Chye, P. R. Skeath, C. Y. Su, and I. Lindau, J. Vac. Sci. Technol. **16**, 1427 (1979); **17**, 1019 (1980).

6 W. E. Spicer, D. J. Friedman, and G. P. Carey, J. Vac. Sci. Technol. A **6**, 2746 (1988).

7 R. H. Williams and M. H. Patterson, Appl. Phys. Lett. **40**, 484 (1982).

8 T. P. Humphreys, M. H. Patterson, and R. H. Williams, J. Vac. Sci. Technol. A **17**, 886 (1970).

9 P. John, T. Miller, T. C. Hsieh, A. P. Shapiro, A. L. Wachs, and T.-C. Chiang, Phys. Rev. Lett. **46**, 838 (1981).

10 D. J. Friedman, I. Lindau, and W. E. Spicer, Phys. Rev. B **37**, 731 (1988).

11 J. L. Shaw, R. E. Viturro, L. J. Brillson, D. Kilday, and G. Margaritondo, J. Vac. Sci. Technol. A **6**, 2752 (1988).

12 G. P. Carey, A. K. Wahi, D. J. Friedman, C. K. Shih, and W. E. Spicer, J. Vac. Sci. Technol. A **6**, 2736 (1988).

13 K. C. Mills, *Thermodynamic Data for Inorganic Sulphides, Selenides and Tellurides* (Butterworths, London, 1974).

14 The heat of formation of PdTe is estimated to be -9.0 kcal/mol

15 J. F. McGilp, J. Phys C **17**, 2249 (1984).

16 J. F. McGilp and I. T. McGovern, J. Vac. Sci. Technol. B **3**, 1641 (1985).

17 A. R. Miedema, P. F. de Châtel, and F. R. de Boer, Physica B **100**, 1 (1980).

18 D. J. Friedman, G. P. Carey, C. K. Shih, I. Lindau, W. E. Spicer, and J. A. Wilson, J. Vac. Sci. Technol. A **4**, 1977 (1986).

19 D. J. Friedman, G. P. Carey, C. K. Shih, I. Lindau, W. E. Spicer, and J. A. Wilson, Appl. Phys. Lett. **48**, 44 (1986).

20 R. R. Daniels, G. Margaritondo, G. D. Davis, and N. E. Byer, Appl. Phys. Lett. **42**, 50 (1983).

21 G. D. Davis, N. E. Byer, R. A. Riedel, and G. Margaritondo, J. Appl. Phys. **57**, 1915 (1985).

22 G. P. Carey, D. J. Friedman, W. E. Spicer, *to be published.*

23 J. A. Silberman, P. Morgen, I. Lindau, W. E. Spicer, and J. A. Wilson, J. Vac. Sci. Technol. **21**, 154 (1982).

[24] J. A. Silberman, Ph. D. thesis, Stanford University (1986), p. 54 (unpublished).

[25] C. K. Shih and W. E. Spicer, Phys. Rev. Lett. **58**, 2594 (1987).

[26] G. L. Hansen, J. L. Schmit, and T. N. Casselman, J. Appl. Phys. **53**, 7099 (1982).

Figure Captions

Figure 1 PES spectra of the Hg 5d, Cd 4d and Ag 4d core levels showing the movement of the bands of HgCdTe upon Ag contact formation and annealing, where the BE is referenced to E_f. The spectra were taken at 80 eV photon energy to provide maximum surface sensitivity (2-3 atomic layers). At the highest coverage, the Hg and Cd core levels have moved ≈ 0.2 eV to deeper BE, but upon annealing at RT for 1 hr have moved back towards the cleaved position.

Figure 2 He I spectra showing the Hg 5d and Cd 4d core levels for the submonolayer coverages Θ of Al. The BE is referenced to E_f. The bands move to deeper BE even at the lowest coverages and remain at this position for all subsequent coverages. The position of the bands correlates to the E_f lying ≈ 0.6 eV above the VBM.

Figure 3 He I spectra of the Hg 5d and Cd 4d shallow core levels as a function of Pd overlayer coverage Θ in ML, where the BE is referenced to the E_f. The bands bend to deeper BE at the lowest coverage and move back slightly towards the cleave position with increasing coverage. Dissociated Hg and alloyed Cd are observed at the higher coverages, indicating that chemistry and intermixing are occuring as more Pd is deposited.

Figure 4 The movement of the E_f at the Ag, Al, and Pd/HgCdTe interfaces grown at 100 K. From the initial position observed at the cleave, the E_f moves into the CB for each interface to approximately 0.6 ± 0.1 eV above the VBM, and this movement is correlated with the interface having little or no disruption. Upon disruption, the E_f moves towards the position observed for the RT cases, and for the Al (*n*-type) and Ag (*p*-type) interfaces, toward a position consistent with the metal doping the

semiconductor. Also shown are is the position of the CBM for the x-values of HgCdTe studied.

Figure 5 Surface band diagrams for the cases shown here. For the "ideal" interface, the Fermi level at the surface moves into the CB for each system, making the surface degenerate n-type. At the disrupted interface, the E_f moves to a position consistent with the doping of the HgCdTe with the overlayer metal. It is interesting to note, that even metals of relatively high EN, Pd (2.2) and Ag (1.9), the E_f moves into the CB at the ideal interface.

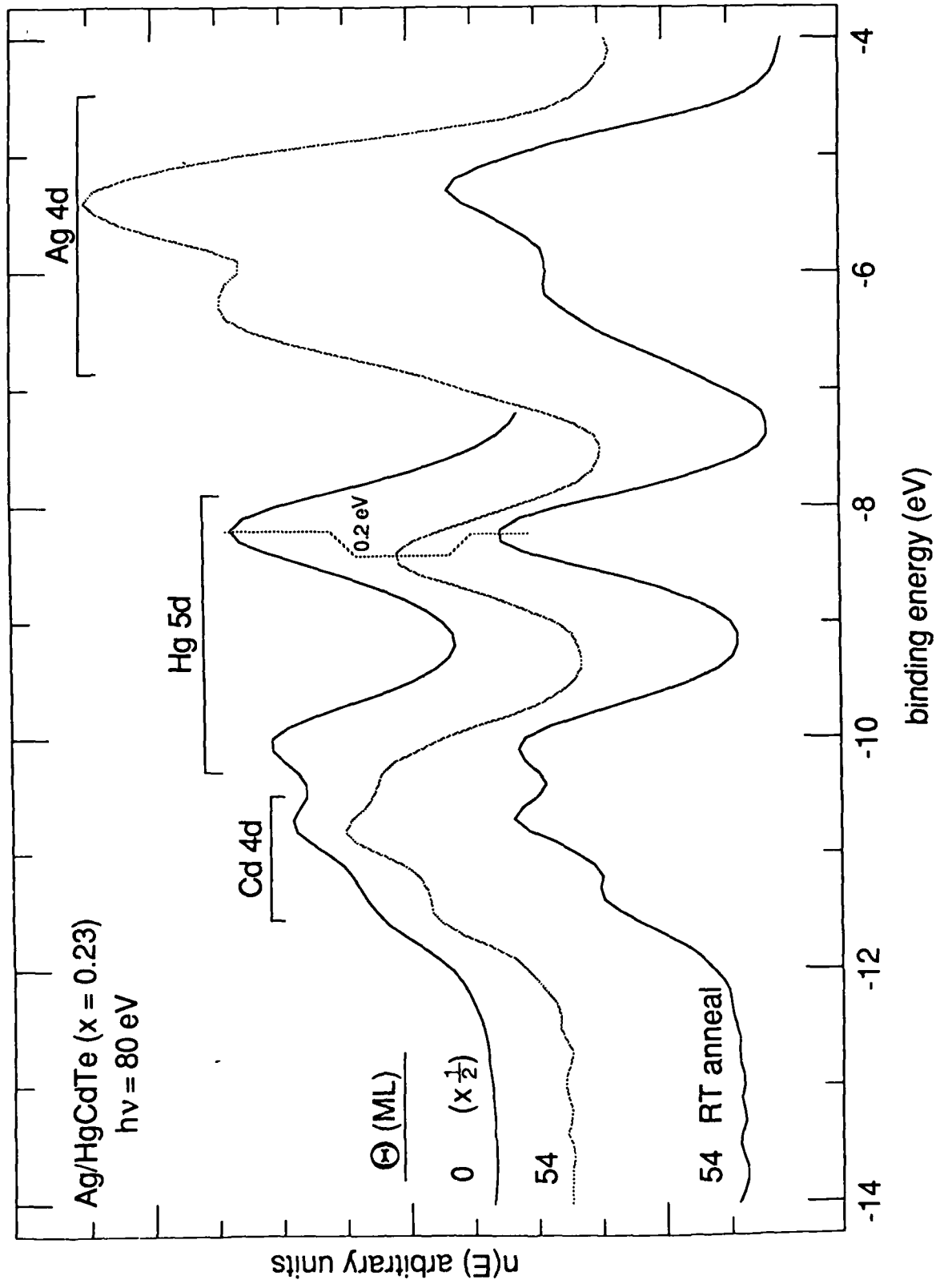
Ag/HgCdTe (x = 0.23)
hν = 80 eV
Θ (ML)
0 (x ½)
54
54 RT anneal
Cd 4d
Hg 5d
Ag 4d
0.2 eV
n(E) arbitrary units
binding energy (eV)
-4
-6
-8
-10
-12
-14

Figure 1

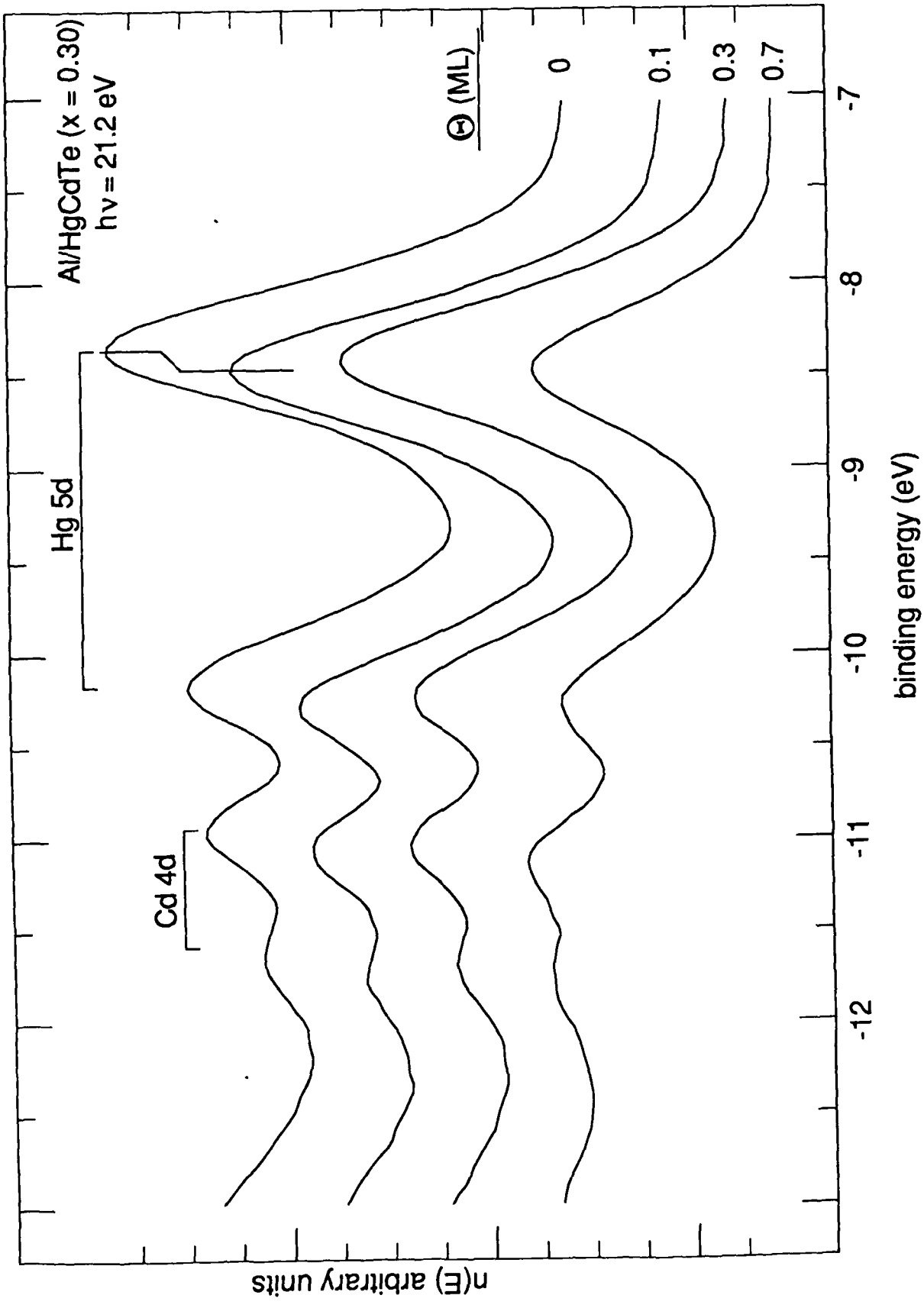
Al/HgCdTe (x = 0.30)
hv = 21.2 eV
Θ (ML)
0
0.1
0.3
0.7
Hg 5d
Cd 4d
-7
-8
-9
-10
-11
-12
binding energy (eV)
n(E) arbitrary units

Figure 2

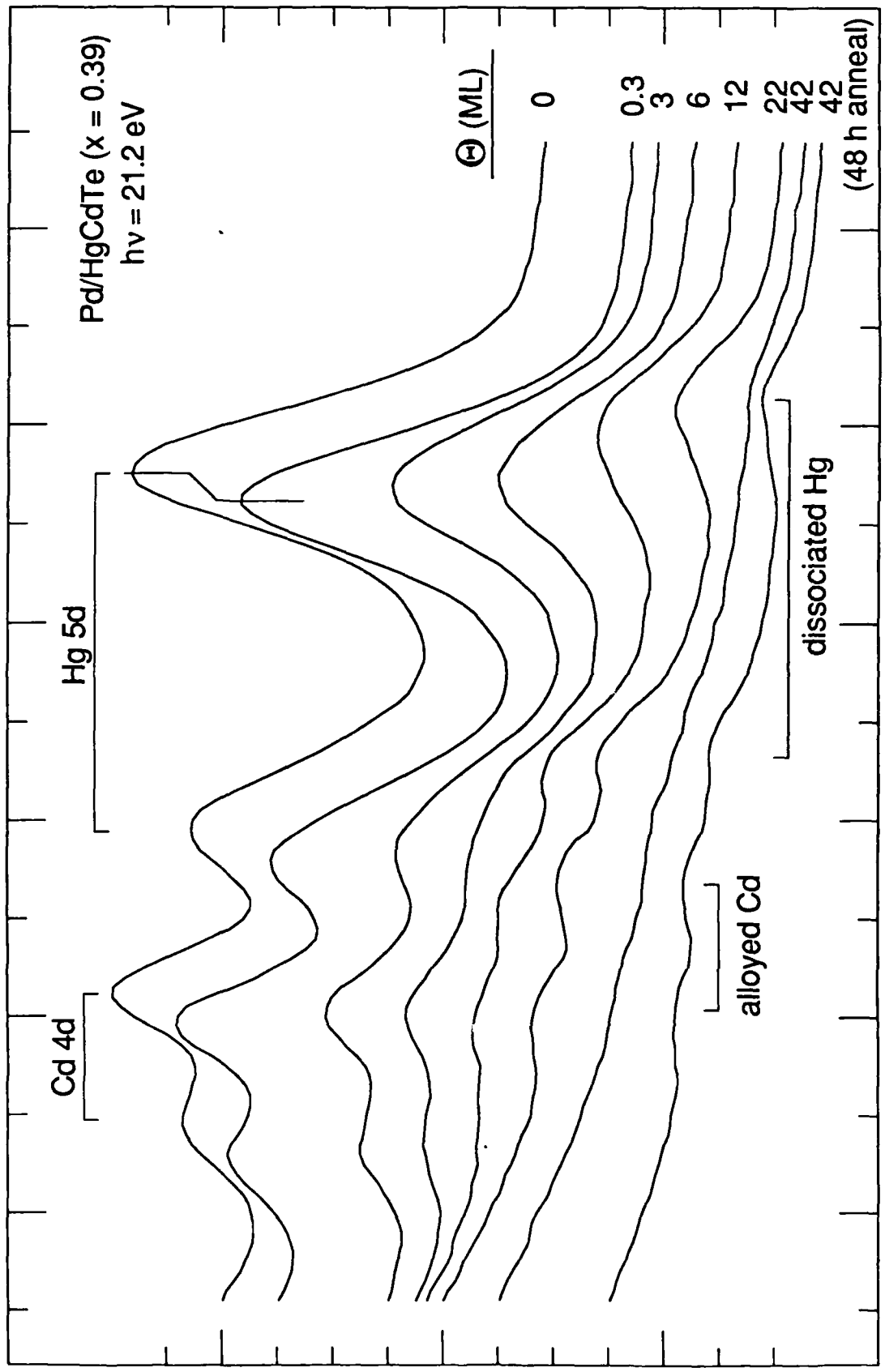
Pd/HgCdTe (x = 0.39)
hν = 21.2 eV
Θ (ML)
0
0.3
3
6
12
22
42
42
(48 h anneal)
Hg 5d
Cd 4d
alloyed Cd
dissociated Hg
-7
-8
-9
-10
-11
-12
binding energy (eV)
n(E) arbitrary units

Figure 3

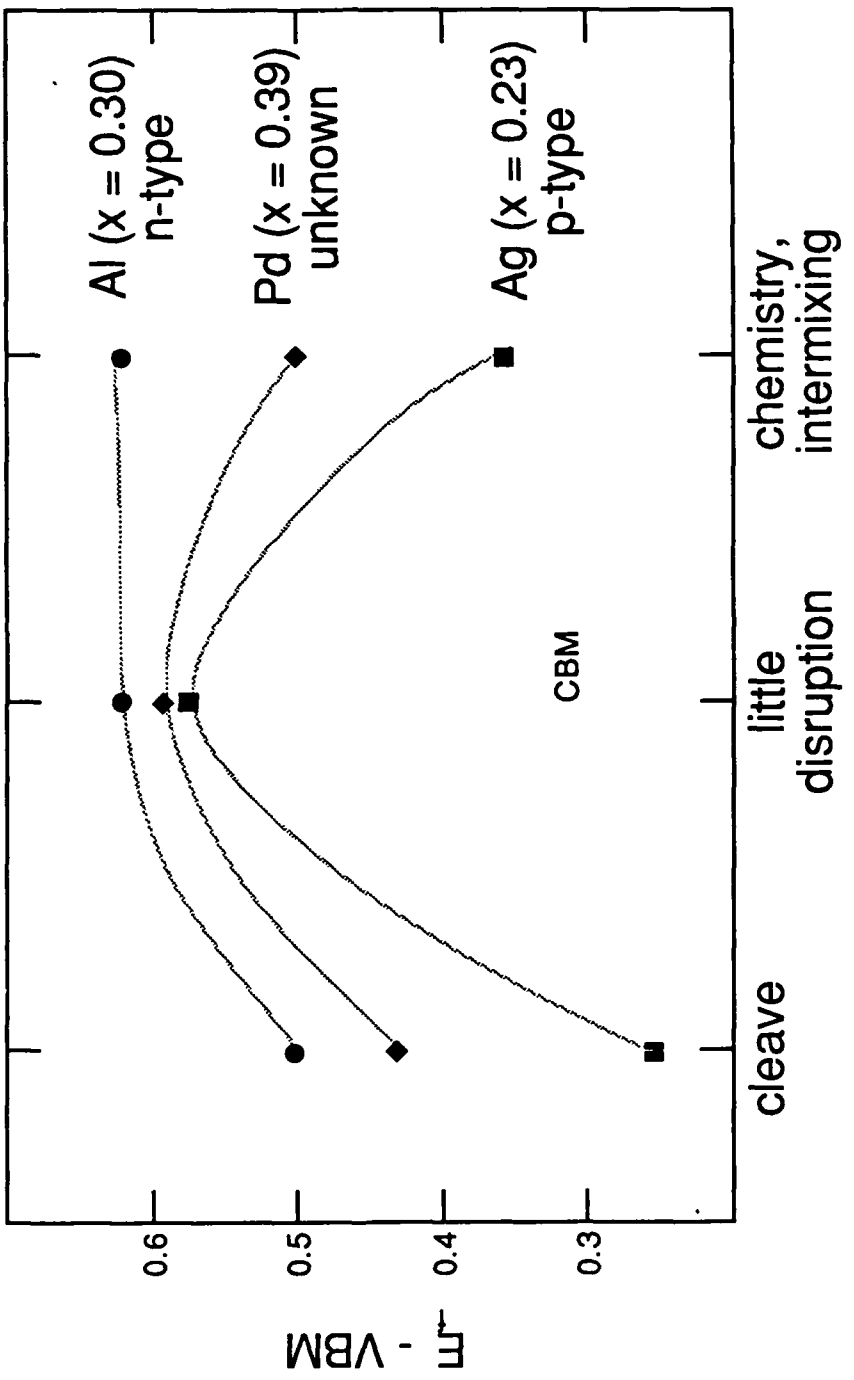
Al (x = 0.30)
n-type
Pd (x = 0.39)
unknown
Ag (x = 0.23)
p-type
CBM
cleave
little
disruption
chemistry,
intermixing
0.6
0.5
0.4
0.3
E_F - VBM

Figure 4

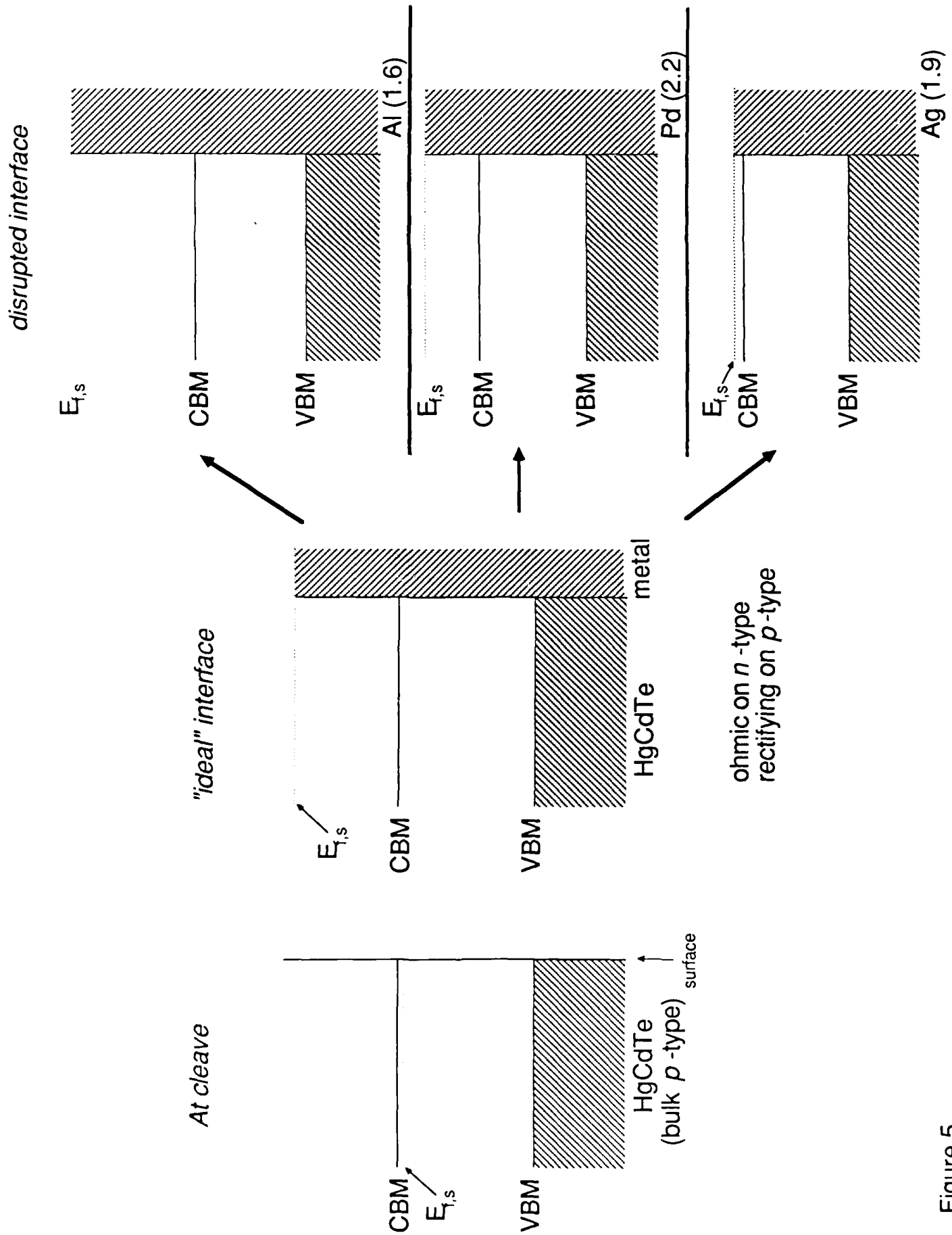
disrupted interface
Al (1.6)
Pd (2.2)
Ag (1.9)
$E_{f,s}$
CBM
VBM
"ideal" interface
metal
HgCdTe
ohmic on *n* -type
rectifying on *p* -type
At cleave
HgCdTe
(bulk *p* -type)
surface

Figure 5

Section III - CdTe and ZnTe Metal Interface Formation and Fermi Level Pinning

I. Introduction

Studies of metal/HgCdTe interface formation have pointed to the weak Hg bonding in HgCdTe as an important factor contributing to the significant semiconductor disruption and metal-semiconductor intermixing that occurs when metals are deposited onto surfaces of UHV-cleaved HgCdTe[1]. Hg depletion ranging from 20 to 60% from the near-surface region after deposition of only a few monolayers (ML) of metal is typically observed. The resulting disruption and interfacial instabilities at metal contacts to HgCdTe prove deleterious to device stability and performance. The related alloy HgZnTe has been proposed as a substitute IR detector material[2] with potentially greater lattice stability than HgCdTe, and it is therefore of interest to compare the behavior of metal contacts to both alloys.

We have studied metal interfaces formed on CdTe and ZnTe in order to investigate interfacial morphology in conjunction with Fermi level pinning behavior at metal coverages from submonolayer to tens of monolayers. Studying the behavior of these related binary semiconductors where the effects of Hg loss are absent gives insight into the role of the weak Hg-bonding in the alloy. Fermi level pinning positions in the binaries are also used[3] to predict and make comparisons between electrical properties of metal contacts to the alloys HgCdTe and HgZnTe.

We focus on the metals Al, Ag, and Pt, chosen to provide a range of reactivities with the substrate. The relevant bulk thermodynamic parameters for interfaces with these metals provide a useful guide for predicting the interfacial chemistry that might be observed, and, in general for metal/HgCdTe systems, the chemistry observed has been consistent with these predictions. Al is highly reactive with Te (ΔH_f,Al_2Te_3 = -76.1 kcal/mol) and Ag and Pt comparatively non-reactive with Te (ΔH_f,Ag_2Te and ΔH_f,PtTe = -8.6 and -10.0 kcal/mol, respectively)[4]. For both Al and Ag, calculations using the semi-empirical model of Miedema[5] predict a minimal driving force for cation (Cd or Zn) alloying with the overlayer metal, whereas strong cation alloying behavior with

Pt is expected[6]. Because of the similar heats of formation for CdTe and ZnTe (ΔH_f,CdTe = -24.1 kcal/mol and ΔH_f,ZnTe = -28.5 kcal/mol), the interfacial chemistry and morphology for each of these metals on both semiconductors is expected to be similar. In comparison to CdTe, the weak Hg bonding in HgCdTe (reflected in the small ΔH_f, HgTe = -7.6 kcal/mol) and consequent ease of Hg loss is expected to result in more disruptive interfaces. Here we emphasize interface morphology for Al/CdTe and Al/ZnTe. We find a case where significantly greater intermixing occurs in CdTe than seen on HgCdTe. The Al/ZnTe interface is also more abrupt than Al/CdTe. We also present band bending results for interfaces of all three metals with p-CdTe and p-ZnTe and consider implications for metal/HgZnTe interface formation.

II. Experimental Procedure

Single crystal bars of CdTe (both p- and n-type) and p-ZnTe (ZnTe obtained from Cleveland Crystals, Inc.),with cross-sectional areas of 5 x 5 mm^2 for CdTe and 2.5 x 2.5 mm^2 for ZnTe, were introduced into a previously baked UHV chamber and then cleaved in vacuum (with base pressure < 1 x 10^{-10} torr) to reveal atomically clean (110) surfaces. Sequential metal depositions were performed by evaporation from a tungsten filament, with metal coverage monitored using a quartz oscillator. Experiments were performed at the Stanford Synchrotron Radiation Laboratory using synchrotron radiation with photon energies chosen for maximum surface-sensitivity, and also using conventional x-ray (Mg Kα and Zr Mζ, hv = 1253.6 and 151.4 eV, respectively) and ultraviolet (He I and II, 21.2 and 40.8 eV) photon sources to provide both surface-sensitive (~7 - 10 Å photoelectron escape depth) and bulk-sensitive (~20 - 25 Å) core level emission. The kinetic energy of photoemitted electrons was measured using a double-pass CMA. In addition, LEED was performed on some of these interfaces in order to monitor surface crystallinity during overlayer growth, with beam current $\leq$ 1 μA. Throughout the following, metal coverages are given in terms of a monolayer (ML), equivalent to the surface density of atoms on the (110) faces

of CdTe or ZnTe (6.74×10^{14} and 7.60×10^{14} atoms/cm^2, respectively). For example, 1 ML corresponds to 1.12 Å of Al on CdTe and 1.26 Å of Al on ZnTe.

III. Results

A. Interfacial Chemistry and Morphology: Al/CdTe and Al/ZnTe

As expected, a strong Al-Te reaction is seen for Al on CdTe and ZnTe, as has been seen in previous studies of the Al/HgCdTe interface[7-8]. A reacted Al-Te layer is formed, and at higher coverages metallic Al forms on top of this reacted region. While the same general chemical behavior is seen for all three systems, significant differences in morphology are seen, with the extent of this reaction on CdTe significantly greater than on either ZnTe or HgCdTe. Figure 1 shows the evolution of the Al 2p core level with Al coverage for Al on n-CdTe and p-ZnTe. On both CdTe and ZnTe, Al emission first emerges with higher binding energy than bulk Al metal, and this reacted Al component moves to still higher binding energy with successive Al depositions. A corresponding shifted component of Te emission, which would be indicative of a reacted Te species distinguishable from Te in bulk CdTe or ZnTe, is not seen; however, a broadening of the Te signal is observed, similar to what is seen for Al/HgCdTe. Furthermore, as described below, while Cd is not incorporated into the overlayer as it forms, Te attenuation from the surface region is very slow. We therefore ascribe this reacted Al 2p signal to Al reacted with Te, with Te retaining the same binding energy as in bulk CdTe (and ZnTe). At higher coverages metallic Al forms on top of this reacted layer, with a signal from unreacted Al emerging at approximately 2.5 eV lower binding energy, corresponding to the binding energy of metallic Al[9]. The emergence of metallic core level emission is accompanied by the appearance of Fermi level emission. On ZnTe, unreacted Al is first seen near 7 ML coverage, compared with its first appearance on HgCdTe after deposition of about 3 ML Al. On CdTe, however, only Al reacted with Te is seen up to near 40 ML on the n-type sample. (On the p-type CdTe, only reacted Al was seen up to the maximum coverage studied of 29 ML.) The dominance of the reacted Al component up to the highest

coverages in CdTe suggests a strong Al reaction with a high degree of Al - Te intermixing, especially in comparison to what is seen for HgCdTe. The separation in binding energy of the reacted and metallic Al components is similar to what has been observed for Al on CdS[10]. Significantly, the observed separation is greater than observed for HgCdTe, where the binding energy of the reacted Al component is only 1 to 1.5 eV higher than the metallic component[7-8]. Thus the reacted Al on HgCdTe emerges with intermediate binding energy which suggests that a less highly reacted species of reacted Al is formed on the alloy.

As Figure 1 shows for CdTe and ZnTe, a strong reacted Al component is present in the surface-sensitive emission (i.e., from within the top 10 Å) at even the highest metal coverages. This observation suggests that a floating layer of reacted Al - Te remains on the surface. Such a surface-segregated layer has been suggested for Al/HgCdTe[7-8]. Further evidence that this layer exists on CdTe is shown in Table I, which compares surface-sensitive (using Zr Mζ, hν = 151.4 eV) and bulk-sensitive (using Mg Kα, hν = 1253.6 eV) Al 2p emission for the higher coverages. The bulk sensitive emission emerges with kinetic energy near 1176 eV, which corresponds to an electron escape depth of about 25 Å; while most of the surface-sensitive emission (shown in Figure 1) emerges from within the top 10 Å. The clear distinction between the metallic and reacted Al 2p peaks makes it possible to separate the reacted and unreacted contributions to the Al 2p signal, with accuracy estimated to be within 30%. Table I gives the percent of the total Al 2p signal which is metallic for both the surface-sensitive and bulk-sensitive emission. It can be seen that the ratio of metallic Al intensity to the reacted Al intensity is greater in the more bulk-sensitive emission. Thus, there is a gradient in metallic Al concentration, with the outer surface rich in reacted Al and the amount of metallic Al increasing as one moves from the outer surface towards the substrate. The floating reacted layer here has been easy to observe more directly than in the case of Al on HgCdTe due to the thickness of the reacted layer formed on CdTe and the greater separation in binding energy between the reacted and unreacted Al 2p components.

Figure 2 shows the attenuation of core levels as a function of Al coverage for Al/n-CdTe. The Te 4d and Cd 4d emission is surface-sensitive, emerging from within the top 7 - 10 Å of the surface. While Te4d emission in the surface region attenuates very slowly with coverage, the Cd intensity drops with coverage as one would expect due to attenuation through a uniform overlayer, with an effective electron escape depth of approximately 10 Å. The bulk Cd/Te ratio, however, does not change appreciably as more metal is deposited. That the Cd/Te ratio at the surface (within the top 10 Å) decreases, while the overall Cd/Te ratio remains unchanged to within a depth of 25Å, suggests that Cd is being rejected from the near surface region and that a Cd-rich layer is built up beneath the reacted overlayer. (If Cd were being lost from the surface to vacuum, which would not be expected from its low vapor pressure, a decrease would be expected in the bulk Cd/Te ratio.) While rejection of Cd from the overlayer would be expected to result in a Cd attenuation rate that is faster than observed, there is evidence of initial islanding of Al on the surface found in the LEED pattern, which persists beyond 5 ML Al coverage, disappearing at 10 ML. Initial islanding of Al on the surface would lead to a slower Cd attenuation than seen seen here, and it is possible that these two effects on the Cd attenuation rate could compensate to give the appearance of an "abrupt" interface with respect to Cd.

A surprising result of this work is the lack of a signal from dissociated Cd that is clearly distinguishable from that of bulk CdTe. For example, Patterson and Williams[12] have reported the appearance of metallic Cd for thick overlayers of Al on CdTe, although they do not give quantitative values of thickness. For the thickness range studied here (up to 81 ML of Al), it did not appear. Although no clear evidence has been seen for elemental Cd forming at the Al/HgCdTe interface, the binding energy of any formed would not necessarily be separated from Cd in bulk HgCdTe[13]. However, on CdTe, a signal from any elemental Cd should be clearly resolvable, emerging with a binding energy of 10.6 eV relative to the Fermi level[9]. Emission from any Cd alloyed with the overlayer would be expected to emerge with about 0.15 eV higher binding energy than elemental Cd[6]; and, though this might not be easily distinguished from metallic Cd, it also

should be clearly resolvable from Cd in bulk CdTe. However, as Figure 3 shows for the Cd 4d core level, a signal from metallic Cd or Cd alloyed with Al is not observed, and neither is it seen in the more bulk-sensitive Cd 3d emission. (The observed shift of the Cd 4d emission with Al deposition in Figure 3 is due to band bending.) Bulk thermodynamics does not favor alloying of Cd with the overlayer. A clear signal from Cd alloyed with the overlayer has been seen in systems where the cation exhibits strong alloying with the overlayer, e.g., for Pt and Cu overlayers on HgCdTe[14] and CdTe[11], respectively.

Although the details of the Al reaction, with the formation of a surface-segregated reacted layer on top of an eventually metallic overlayer, are essentially the same in both CdTe and ZnTe, the extent of this reaction on CdTe is significantly greater. A decrease in the ratio of cation Cd or Zn intensity to that of Te from the near surface is seen for both CdTe and ZnTe. However, a saturation in the decrease in the Zn/Te ratio occurs near the coverage where metallic Al is first seen, suggesting that the rejection of Zn from the overlayer slows when metallic instead of reacted Al forms.

B. Band Bending

In Table II we give our measured values for the final surface Fermi level pinning positions relative to the valence band maximum, $E_{fi} = E_f - E_{vbm}$, for the metals Al, Ag, and Pt on vacuum-cleaved surfaces of p-type CdTe and p-type ZnTe. The movement of the Fermi level relative to the VBM is determined by shifts in the core levels, which can be measured very precisely, as a function of metal coverage. The VBM position for CdTe is then located 10.25 ± 0.05 eV above the position of the Cd $4d_{5/2}$ core level, and the ZnTe VBM is located 9.75 ± 0.05 eV above the position of the Zn 3d core level, as determined using angle-resolved photoemission[15]. We find that for CdTe and ZnTe (with very different bandgaps of, for CdTe and ZnTe, $E_g = 1.5$ eV and 2.2 eV, respectively), for each of these metals, the Fermi level pins at roughly the same distance from the VBM in both CdTe and ZnTe. We note in addition that the ZnTe value lies at about 0.2

eV closer to the VBM than CdTe for all three metals. The as-cleaved position of E_f for ZnTe was ~ 0.4 eV above the VBM for all three cleaves; for CdTe, E_{fi} on the cleaved surfaces was about 0.5 eV for the Al and Pt cleaves and 0.65 for the Ag cleave. Upon metal deposition, E_f moves from its position at the cleave up towards the CBM. In the case of Ag/ZnTe, the Fermi level moves up with coverage to 0.8 eV above the VBM and then down to the final position listed in Table II. For Al and Pt, the Fermi level position stabilized below 1 ML coverage for both CdTe and ZnTe. Below we discuss the various models for Fermi level pinning behavior at metal/semiconductor interfaces that might agree with the observed difference in pinning positions. As we will discuss, an interesting point is that the movement of the Fermi level in the reactive Al/CdTe system is complete before the appearance of any metallic Al in the spectra, and therefore effects dependent upon the metallicity of the overlayer appear to be ruled out in this case.

IV. Discussion

A. Al on CdTe, ZnTe, and HgCdTe

The differences seen in the extent of the reaction on CdTe and HgCdTe, and the more highly reacted Al component seen in CdTe compared to HgCdTe, are not explained from a consideration of bulk thermodynamic parameters alone. Since in HgCdTe, a reactive metal such as Al can remove Te from Hg more easily than from Cd or Zn, and rapid Hg loss provides a ready source of Te, a more extensive Al-Te reaction might be expected to occur. Clearly this is not the case. Instead, the kinetics at the HgCdTe interface may be dominated by the disruption due to Hg depletion, determining the extent of reaction and intermixing of semiconductor components with the overlayer metal. For instance, after only a few ML of Al are deposited onto HgCdTe[7-8], at least 50% of the Hg is already lost from the first approximately 30 Å of the substrate surface. Such rapid Hg loss would be expected to result in significant disorder, with possibly a collapse of the lattice. The rapid depletion of Hg from the lattice then slows, to a rate expected for attenuation of the Hg signal through an overlayer[8]. Formation of a barrier to further movement of

semiconductor components due to inhibited diffusion of Hg through the disrupted region can explain the less extensive reacted region seen for Al/HgCdTe in comparison to CdTe.

While the presence of Hg can account for the difference in behavior observed between Al/HgCdTe and Al/CdTe, the difference in behavior between ZnTe and CdTe is surprising, when simple considerations of bulk thermodynamics predict the same behavior for both.

B. Band Bending

From the rough similarity in E_{fi} for CdTe and ZnTe listed in Table II, one would expect for these metals Schottky barriers of roughly the same height on both p-CdTe and p-ZnTe. We note, however, that the ZnTe value lies at about 0.2 eV closer to the VBM than CdTe for all three metals. We speculate on possible models which would be consistent with this result, focussing on the two models most often used to interpret Fermi level movement with metal coverage: the metal-induced gap states (MIGS) model, in which tailing of the metal wavefunctions into the semiconductor produce states in the bandgap that pin the Fermi level; and defect models, in which the defect energy levels responsible for the observed pinning in CdTe and ZnTe would lie at nearly the same energy with respect to the VBM in both semiconductors. The observed difference in pinning positions for CdTe and ZnTe is consistent with MIGS models, which predict that a difference in E_{fi} for two semiconductors will be observed which depends on their band lineup[16], i.e., that the difference in Schottky barrier height for two semiconductors will be given by their valence band offset. The measured ZnTe - CdTe valence band offset has been determined[15] as $0.18 \pm .06$ eV, with the ZnTe VBM lying above that of CdTe, in agreement with what we see here. However, for the case of Al on CdTe and ZnTe, band bending is completed below 1 ML, well before established Fermi level emission and a metallic Al component is seen. Consequently a MIGS-type mechanism, which depends upon the metallicity of the overlayer, appears to be ruled out in this instance, and a defect mechanism is favored. Calculations for bulk defects in the HgTe - CdTe system are available from the work of Kobayashi *et al.*[17]. We focus on defects involving Te in

view of the frequently observed outdiffusion of Te from the lattices of both HgCdTe[7,14,18] and CdTe[11] upon metal deposition. From their work, a likely candidate involved in Fermi level movement in CdTe might be the Te_{Cd} antisite, with an energy about 1 eV above the VBM. This defect could account for the observed narrow range of Fermi level pinning positions ranging from 0.7 - 1.1 eV above the VBM seen for CdTe[11]. Alternatively, a possibility for an intrinsic defect which might be involved is the Te vacancy, which is predicted to be a shallow double donor in CdTe[19]. Comparison with ZnTe is hampered by the lack of available calculations specifically for this system, however one might speculate that similar defects occur here as well. Although extensive work is reported in the literature for Schottky barrier heights and Fermi level pinning positions for a wide range of metals on CdTe, there is a lack of available theoretical work on surface defects in II-VI materials. Clearly a much greater understanding is desirable.

One can extrapolate from the Fermi level pinning position in the binaries through the range of alloy compositions $Hg_{1-x}Cd_xTe$ and $Hg_{1-x}Zn_xTe$ to obtain predictions for the electrical behavior of metal/HgCdTe and metal/HgZnTe interfaces. Several different models for Fermi level pinning may be used, as discussed by Spicer *et al.*[3], and these yield similar predictions, that ohmic contacts will be obtained for metals on n-type HgCdTe below a certain x-value of about 0.4, and that rectifying contacts will be obtained on p-type HgCdTe of all compositions. The observed similarity of E_{fi} for CdTe and ZnTe lead to a prediction that metal contacts to the alloy HgZnTe would yield in principle the same properties as on HgCdTe, that is, intrinsically ohmic contacts will be obtained on n-type HgZnTe below a certain x-value, with perhaps a lower crossover of x = 0.3 due to the larger bandgap of HgZnTe, and rectifying contacts will be obtained on p-type HgZnTe of all compositions. For Fermi level pinning in the Hg-containing alloys, however, additional mechanisms for Fermi level movement are possible that are not present in CdTe and ZnTe which involve Hg loss. These mechanisms involve metal movement into the semiconductor via Hg vacancies, and the resultant doping of the substrate[6,20].

V. Conclusions

In summary, the Al, Ag, and Pt interfaces with CdTe and ZnTe have been investigated in a comparative study of CdTe and ZnTe metal interface morphology and Fermi level pinning behavior. For reactive Al overlayers, we find a case where a more disruptive interface with a higher degree of intermixing occurs in the binary CdTe than has been seen for the Al/HgCdTe interface. The extent of the Al reaction with Te is inhibited in the Hg-containing alloy due to the disruption due to Hg loss. The Fermi level pinning positions, E_f - E_{vbm}, for Al, Ag, and Pt on p-type CdTe and p-ZnTe are found to be roughly the same, with the values for ZnTe lying about 0.2 eV closer to the VBM for each metal. From these results, similar behavior for metal contacts to the alloys HgCdTe and HgZnTe is expected.

Acknowledgment:

*Work partially supported by DARPA under contract # N00014-86-K0854.

References

a) Stanford Ascherman Professor of Engineering.

1. D. J. Friedman, G. P. Carey, I. Lindau, W. E. Spicer, and J. A. Wilson, J. Vac. Sci. Technol. B **4**, 980 (1986).
2. A. Sher, A.-B. Chen, W. E. Spicer, and C.-K. Shih, J. Vac. Sci. Technol. A **3**, 105 (1985).
3. W. E. Spicer, D. J. Friedman, and G. P. Carey, J. Vac. Sci. Technol. A **6**, 2746 (1988).
4. K. C. Mills, Thermodynamic Data for Inorganic Sulfides, Selenides, and Tellurides (Butterworths, London 1974).
5. A. R. Miedema, P. F. Chatel, and F. R. de Boer, Physica B **100**, 1 (1980).
6. D. J. Friedman, G. P. Carey, I. Lindau, and W. E. Spicer, J. Vac. Sci. Technol. A **5**, 3190 (1987). Calculations of the heat of solution of cation Cd and Hg at infinite dilution in metal M for several metals obtained using the Miedema model (ref. 5 with tabulations therein) are given here. To these we add values ΔH_{sol}(Zn;M) for Zn: Al, +0.5 kcal/mol; Ag, -4.3 kcal/mol; Pt, -30.0 kcal/mol.
7. G. D. Davis, N. E. Byer, R. A. Riedel, and G. Margaritondo, J. Appl. Phys. **57**, 1915 (1985).
8. D. J. Friedman, G. P. Carey, C. K. Shih, I. Lindau, W. E. Spicer, and J. A. Wilson, J. Vac. Sci. Technol. A **4**, 1977 (1986).
9. L. Ley and M. Cardona, Eds., Photoemission in Solids II (Springer-Verlag, Berlin 1979).
10. L. J. Brillson, R. S. Bauer, R. Z. Bachrach, and J. C. McMenamin, J. Vac. Sci. Technol. **17**(1), 476 (1980).
11. D. J. Friedman, I. Lindau, W. E. Spicer, Phys. Rev. B **37**, 731 (1988).
12. M. H. Patterson and R. H. Williams, J. Cryst. Growth **59**, 281 (1982).
13. D. J. Friedman, Ph. D. Thesis, Stanford University, 1987.
14. D. J. Friedman, G. P. Carey, I. Lindau, W. E. Spicer, Phys. Rev. B **35**, 1188 (1987).

15. C. K. Shih, A. K. Wahi, I. Lindau, and W. E. Spicer, J. Vac. Sci. Technol. A **6**, 2640 (1988).

16. J. Tersoff, Phys. Rev. Lett. **56**, 2755 (1986).

17. A. Kobayashi, O. F. sankey, and J. D. Dow, Phys. Rev. B **25**, 6367 (1982).

18. A. Franciosi, P. Philip, and D. J. Peterman, Phys. Rev. B **32**, 8100 (1985).

19. M. S. Daw, D. L. Smith, C. A. Swarts, and T. C. McGill, J. Vac. Sci. Technol. **19** (3), 508 (1981).

20. G. P. Carey, A. K. Wahi, D. J. Friedman, C. E. McCants, and W. E. Spicer, Proceedings of the 1988 HgCdTe Workshop, J. Vac. Sci. Technol., to be published.

Table I. The percent of the total Al 2p signal which is metallic. The bulk-sensitive data was taken with XPS using Mg Kα.

Al coverage (ML)	bulk (25 Å)	surface (10 Å)
23	0 %	0 %
46	60 %	45 %
81	79 %	67 %

Table II. Final surface Fermi level pinning positions relative to the valence band maximum, $E_{fi} = E_f - E_{VBM}$, for the metals Al, Ag, and Pt on vacuum cleaved surfaces of p-CdTe and ZnTe.

	p-CdTe	p-ZnTe
Al	1.1 ± .1	0.9 ± .1 eV
Ag	0.85 ± .1	0.65 ± .1 eV
Pt	0.95 ± .1	0.7 ± .1 eV

Figure Captions

Figure 1. Surface sensitive photoemission spectra showing the evolution of the Al 2p core level as a function of Al coverage on (a) ZnTe and (b) CdTe. Most of the signal emerges from within the top 10 Å of the surface. At higher coverages, emission from metallic Al at lower binding energy to reacted Al is seen.

Figure 2. Attenuation of core level intensity as a function of Al coverage for Al on n-CdTe. The Te 4d emission from the surface attenuates very slowly with coverage, with Te reacting with the overlayer metal. The more rapid decrease in Cd 4d intensity indicates Cd is not incorporated into the Al overlayer.

Figure 3. Cd 4d spectra for Al on n-CdTe with increasing Al coverage. The observed shift is due to band bending. No evidence is seen for elemental Cd, with a binding energy of 10.6 eV relative to the Fermi level. Emission from any Cd alloyed with the overlayer would be expected to emerge with 0.15 eV higher binding energy than elemental Cd [ref. 6] and is not observed.

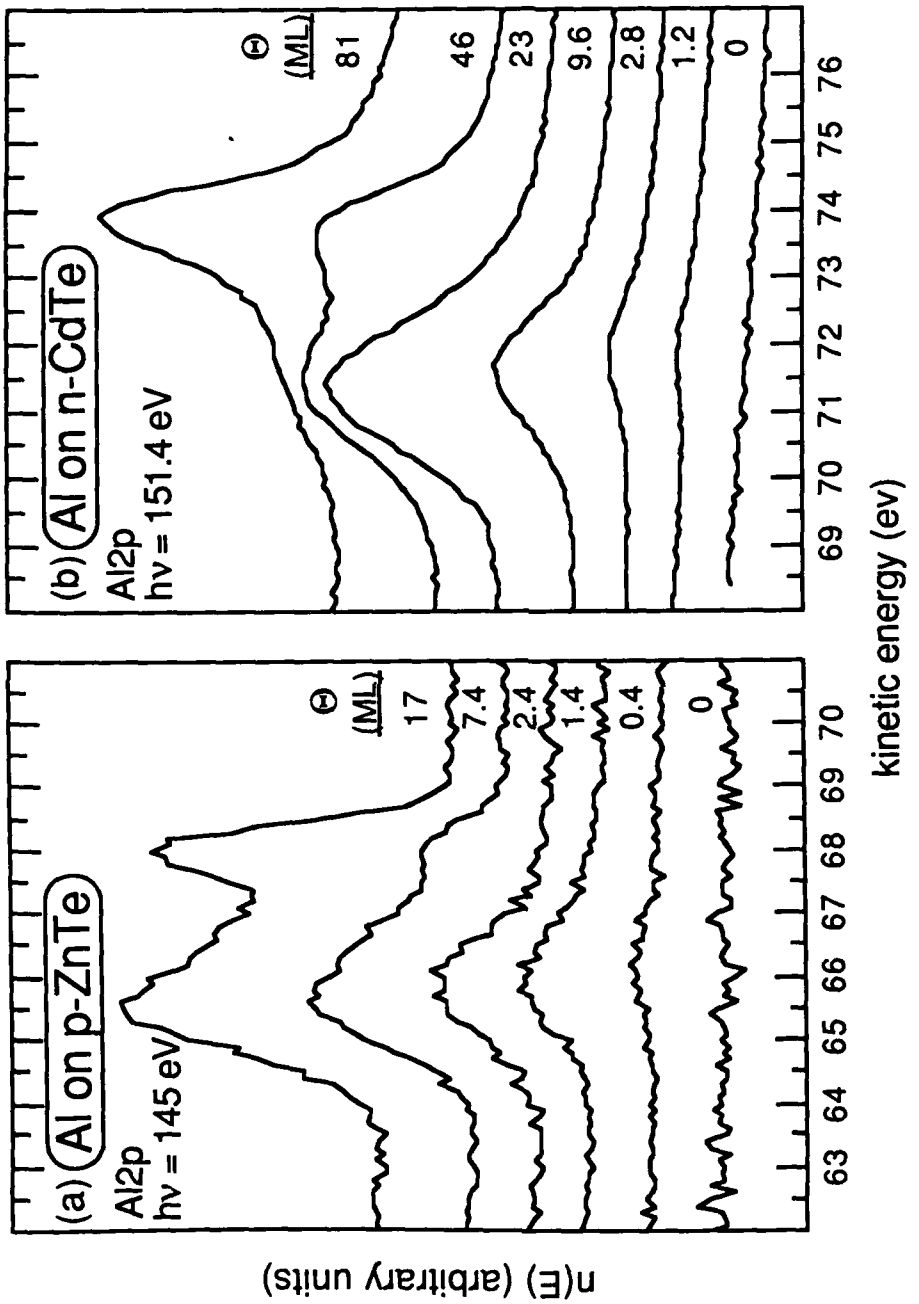
(a) Al on p-ZnTe
Al2p
hν = 145 eV
Θ (ML)
17
7.4
2.4
1.4
0.4
0
63 64 65 66 67 68 69 70
(b) Al on n-CdTe
Al2p
hν = 151.4 eV
Θ (ML)
81
46
23
9.6
2.8
1.2
0
69 70 71 72 73 74 75 76
kinetic energy (ev)
n(E) (arbitrary units)

Figure 1

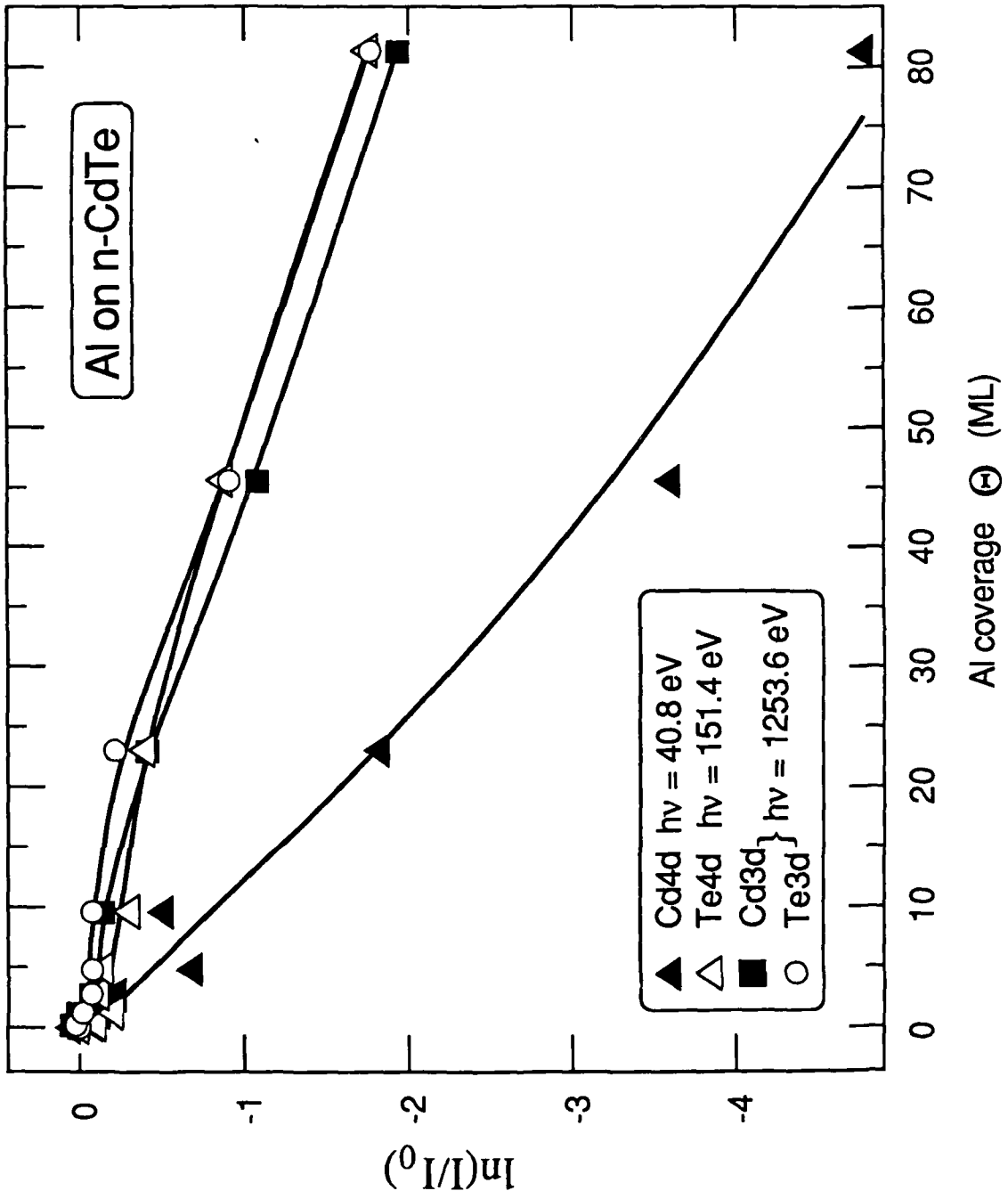
Al on n-CdTe
Cd4d hv = 40.8 eV
Te4d hv = 151.4 eV
Cd3d, Te3d hv = 1253.6 eV
ln(I/I0)
0
-1
-2
-3
-4
0
10
20
30
40
50
60
70
80
Al coverage Θ (ML)

Figure 2

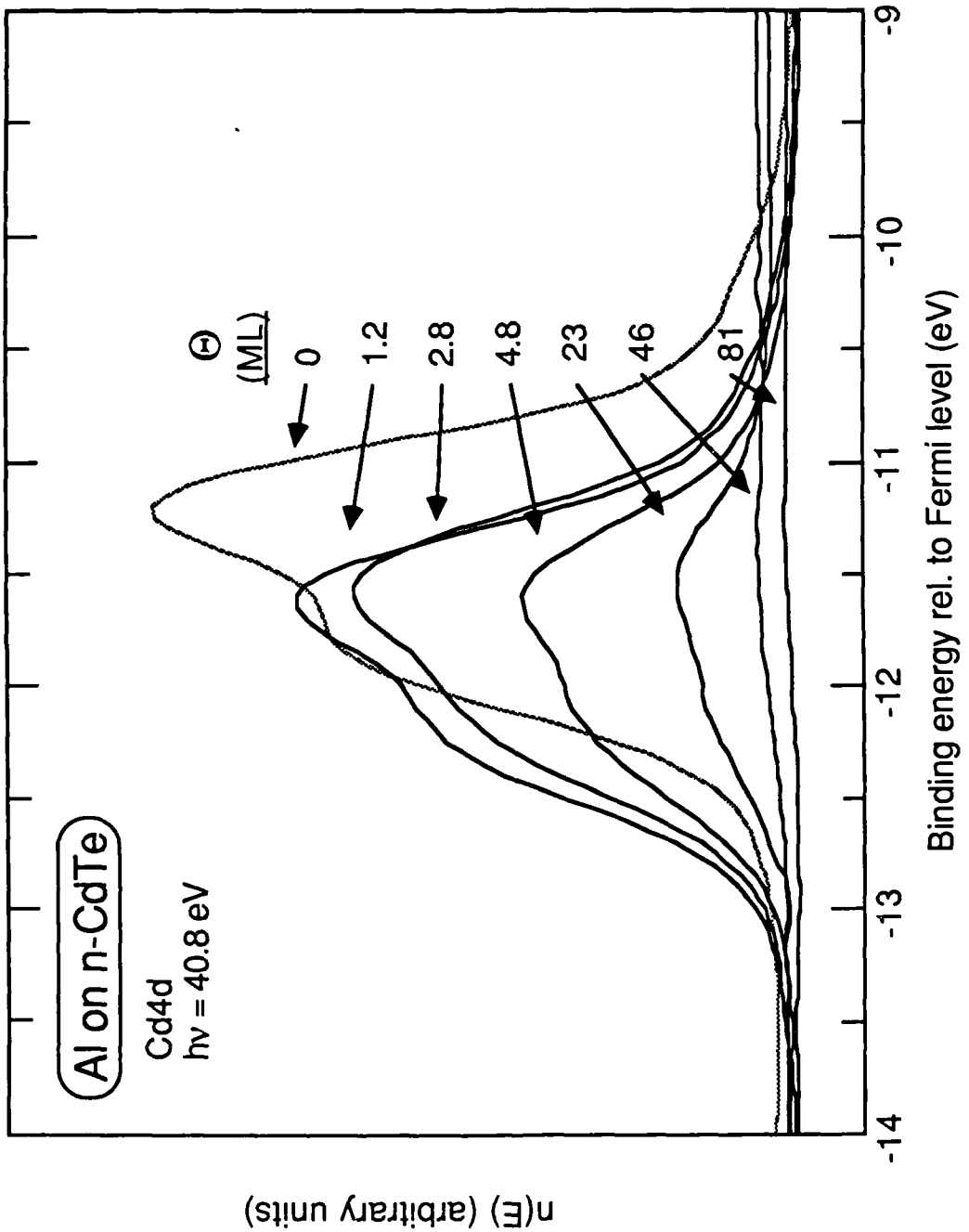
Al on n-CdTe
Cd4d
hν = 40.8 eV
Θ (ML)
0
1.2
2.8
4.8
23
46
81
-9
-10
-11
-12
-13
-14
Binding energy rel. to Fermi level (eV)
n(E) (arbitrary units)

Figure 3

Section IV - Room Temperature Growth of Pd Overlayers on HgCdTe and CdTe

I. Overview

The interface formed in UHV between the HgCdTe substrate held at RT and Pd is among the most complex observed at metal/HgCdTe interfaces. This section describes the experimental evidence for Hg, Cd, and Te dissociation from the HgCdTe substrate during the initial stages of formation of the Pd/HgCdTe (x = 0.39) contact in UHV. The dissociation of all substrate constituents from the substrate and subsequent intermixing into the overlayer has not been observed for any other metal/HgCdTe interfaces reported to date. The heats of alloying between the overlayer metal Pd and the substrate cations are shown to play a dominant role in the interface chemistry. The bulk thermodynamic data between Pd and the HgCdTe constituents indicates that Pd will chemically interact with not only Te from the substrate, but with the cations Cd and Hg as well. Experimental observations at the interface between Pd and CdTe will then be presented in section IV-4, where the difference in interface morphology between the Pd/CdTe and Pd/HgCdTe interfaces are correlated to the presence of the weak Hg-Te bond in the HgCdTe lattice.

II. Introduction

As mentioned above, interfaces formed between metals and HgCdTe are of great interest not only because of the major role they play in the proper manufacture of devices, but the study of such interfaces provides clues into the strength and stability of the HgCdTe lattice itself. The effect of bulk thermodynamic reactivities between overlayer metals and the HgCdTe constituents can be correlated to the morphological and electrical properties of the contact. Of the metal/HgCdTe studies conducted to date, most have concentrated on metals with high reactivity with Te but low reactivity with Cd and Hg. More recently,

metals of high reactivities with the cations have been studied. For example, the interaction between the rare earths Yb and Sm have been reported on by Raisanen [3] and Wall [10], where it is seen that the Hg stays in the vicinity of the surface in the Sm and Yb overlayers and that these overlayers can provide for a thermodynamic and kinetic barrier between the HgCdTe substrate and other reactive overlayers such as Al. Friedman [25] reports on the UHV formed Pt/HgCdTe interface, where spectroscopic evidence of the dissociation of both the substrate Cd and Te is presented along with the observation of Hg loss from the substrate.

These studies have shown that, in addition to considering metal-anion heats of formation, overlayer-cation alloying should also be considered in determining the interface reactivity, as first pointed out by McGilp [26]. Table 4.1 gives relevant thermodynamic data for the metals mentioned above as well as for Ag and Al. The values reported here have been tabulated in part by Friedman [25] and Wall [10]. The heats of metal-telluride and metal-cation formation ΔH_f are provided in Ref. [15], and the heats of alloying $\Delta H_{sol}(C;M)$ between the cations C in infinite dilution in the overlayer metal M are calculated using the semiemperical model of Miedema [27, 28]. The cation core shifts $\Delta E(C;M)$ to deeper BE relative to the pure metallic cation BE for cation C dissolved in infinite dilution in metal M are calculated using the ΔH_{sol} values as described in Ref. [29]. Although the estimated heat of telluride formation (ΔH_f = -9.0 kcal/mol) [Ref. 15] is only moderate for PdTe, the exothermic heats of solution ($\Delta H_{sol}(Cd;Pd)$ = -32.4 kcal/mol, and $\Delta H_{sol}(Hg;Pd)$ = -26.2 kcal/mol) are large. For comparison, the heat of

Table 4.1

Metal (M)	Telluride	ΔH_f(telluride) (kcal/mole)	ΔH_f(MCd) (kcal/mole)	ΔH_f(MHg) (kcal/mole)	ΔH_{sol}(Cd;M) (kcal/mole)	ΔH_{sol}(Hg;M) (kcal/mole)	ΔE(Cd;M) (eV)	ΔE(Hg;M) (eV)
Cd	CdTe	-24.1						
Hg	HgTe	-7.6						
Ag	Ag_2Te	-8.6	-2.4	-1.4	-3.4	-2.1	-0.02	+0.11
Al	Al_2Te_3	-76.2	+1.2	+1.4	+3.4	+4.1	+0.15	+0.32
Pd	PdTe	-9.0	-24.4	-18.6	-32.4	-26.2	-0.54	-0.39
Pt	PtTe	-10.0	-18.6	-12.0	-24.4	-16.4	-0.42	-0.22
Sm	SmTe	-74	-29.3	-35.3	-33.7	-41.3	...	...

Table 4.1: The experimental and calculated thermodynamic parameters of heats of metal-telluride and metal-cation formation ΔH_f, heats of solution ΔH_{sol}(C;M) of cation C in metal M, and cation core shifts ΔE(C;M) to deeper BE relative to the pure metallic cation BE for cation C dissolved in metal M.

PtTe telluride formation (ΔH_f = -10.0 kcal/mol) is comparable and the heats of solution (ΔH_{sol}(Cd;Pt) = -24.4 kcal/mol, and ΔH_{sol}(Hg;Pt) = -16.4 kcal/mol) are slightly less than that of PdTe, but a large difference in the Hg concentration occurs at interfaces formed with the two metals and HgCdTe. Also given in the table are the cation core level shifts to deeper BE from the pure metallic values, where, for the cations dissolved into the overlayer Pd in infinite dilution, ΔE(Cd;Pd) = -0.54 eV and ΔE(Hg;Pd) = -0.39 eV. The large predicted shift of the Cd and Hg core levels upon alloying indicates that unambiguous spectroscopic evidence should arise from the core level spectra if Cd and Hg do alloy into the Pd overlayer. The BE of the Cd $4d_{5/2}$ is -10.6 eV [30] with respect to the E_f for metallic Cd and should shift -0.54 to approximately -10.06 eV upon alloying into Pd, and is approximately -10.9 eV ($E_{Cd4d_{5/2};Hg_{0.61}Cd_{0.39}Te}$ - E_{VBM} + E_f = -10.5 - 0.4 eV) with

respect to the E_f for x = 0.39 HgCdTe, where the BE of the Cd $4d_{5/2}$ as a function of x-value is taken from Ref. [31] and the E_f is assumed to be at the CBM which is 0.4 eV above the VBM for x = 0.39 HgCdTe. Therefore the core level shift expected in going from Cd in HgCdTe to Cd alloyed into the overlayer Pd should be on the order of 0.8 to 0.9 eV to lower BE, which should be clearly resolvable in PES using a He excitation source, and direct spectroscopic evidence for Cd alloyed into the Pd is observed here. As will be shown in the rest of this chapter, the interface properties between Pd and HgCdTe are governed by the reactivities between Pd and the substrate cations Hg and Cd.

III. Pd/HgCdTe results

A. Hg dissociation

Figures 4.8 and 4.9 show He I spectra of the the shallow cores of Hg and Cd and the valence band of HgCdTe as a function of Pd overlayer coverage. There is very little (< 0.05 eV) shift of the spectral features at the lowest coverages, indicating little or no band bending at this interface. The BE of the Hg $5d_{5/2}$ peak at the cleave is measured to be -8.13 ± 0.05 eV, which places the E_f 0.33 eV above the VBM at the cleaved surface, rendering the surface *n*-type, which is commonly observed.

At the 8 ML Pd coverage shown in Fig. 4.8, a shoulder appears to the lower BE side of the Hg $5d_{5/2}$ peak which persists to 75 ML coverage, the highest coverage shown in the figure. At 75 ML, the centroid of the Hg $5d_{5/2}$ peak is at -7.7 eV BE, which matches the BE given in Ref. [30] for metallic Hg. The presence of the Hg signal at this high coverage of Pd indicates that the Hg giving rise to the metallic peak has dissociated from the HgCdTe substrate and moved into the Pd overlayer. Fig 4.10 shows He II spectra of the same BE energy region, which, because of the increased kinetic energy of the escaping electrons, is much more surface sensitive (λ = 4-7 Å versus 15Å for He I). Any

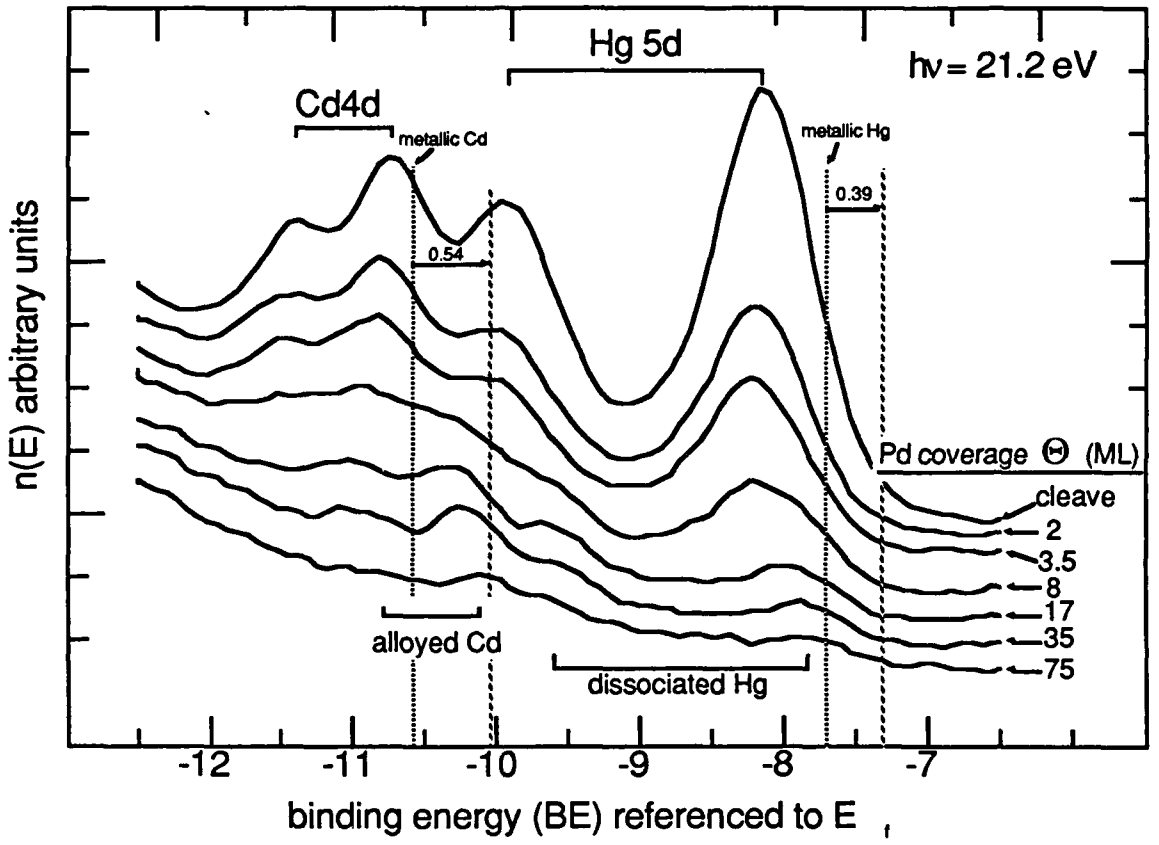

Figure. 4.8. He I spectra of the Hg 5d and Cd 4d shallow core levels versus Pd overlayer coverage. Little or no band bending is observed for the low coverages. At 8 ML coverage, shoulders to the lower BE side of both of the doublets appear. The higher coverage position of the Hg $5d_{5/2}$ peak is close to that of metallic Hg, and the position of the Cd $4d_{5/2}$ is attributed to Cd alloyed into the Pd overlayer.

intensity of the dissociated peak has almost disappeared by the 35 ML coverage, indicating that the residual dissociated Hg is not located at the surface for the highest coverages.

Deconvolution of the substrate and dissociated peaks can provide useful information into the surface morphology. Due to the overlap of the Hg peaks with the Cd 4d's in these spectra, it is difficult to deconvolute the substrate and dissociated contributions to the spectra. Proper deconvolution is afforded by examining the Hg $4f_{7/2}$

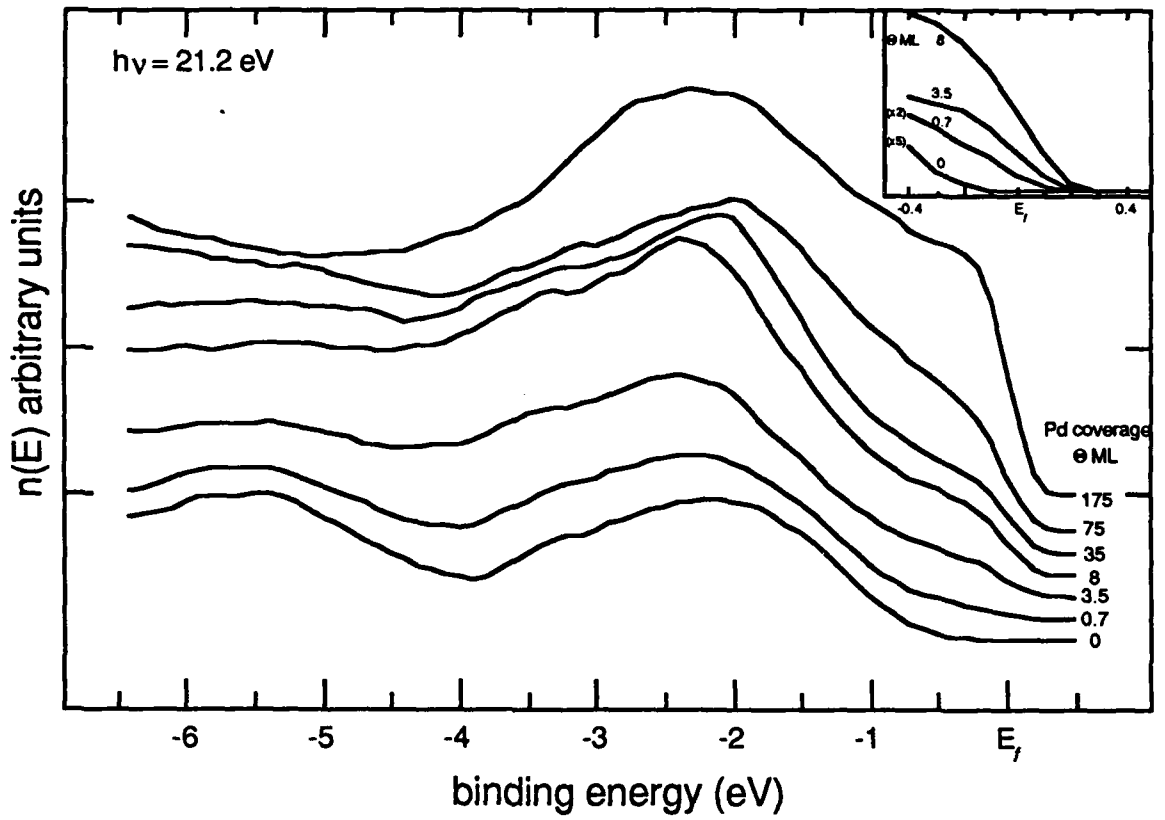

Figure. 4.9. He I spectra of the valence band states versus Pd overlayer coverage. The upper right shows the formation of the Fermi level with coverage, where emission from the Fermi level begins at 0.7 eV, and the completion of the Fermi level is essentially completed by 3.5 ML Pd coverage.

core level shown in Fig. 4.11, where a meaningful deconvolution of the spectra can be performed because of the large separation in the substrate and dissociated peaks and there are no other spectral features overlapping this core level. These spectra were taken at hν = 1253.6 eV, hence the escape depth of the 1150 eV kinetic energy electrons is approximately 20 Å, or close to that expected for the low kinetic energy electrons giving rise to the He I spectra in Fig. 4.8. The deconvolution was performed by free fitting (*i.e.* allowing the width, centroid and intensity of the Lorentzian theoretical line shape vary for

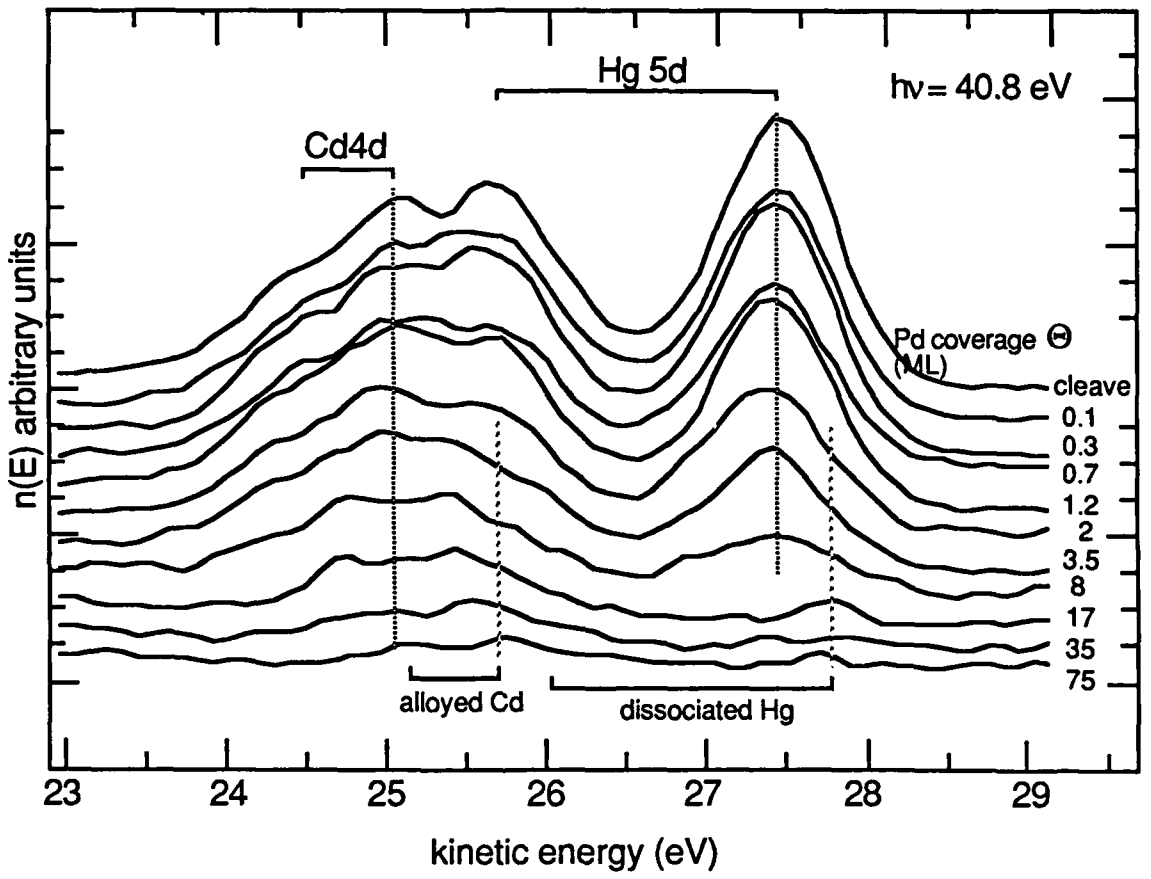

Figure. 4.10. He II spectra of the Hg 5d and Cd 4d cores versus Pd overlayer coverage. The electrons giving rise to this specta have an escape depth of 4 - 7 Å, hence are arising more from the surface than those giving rise to the spectra in Fig. 4.8. Very little elemental Hg is observed at the higher coverages, whereas a small Cd signal is present at the highest Pd coverages.

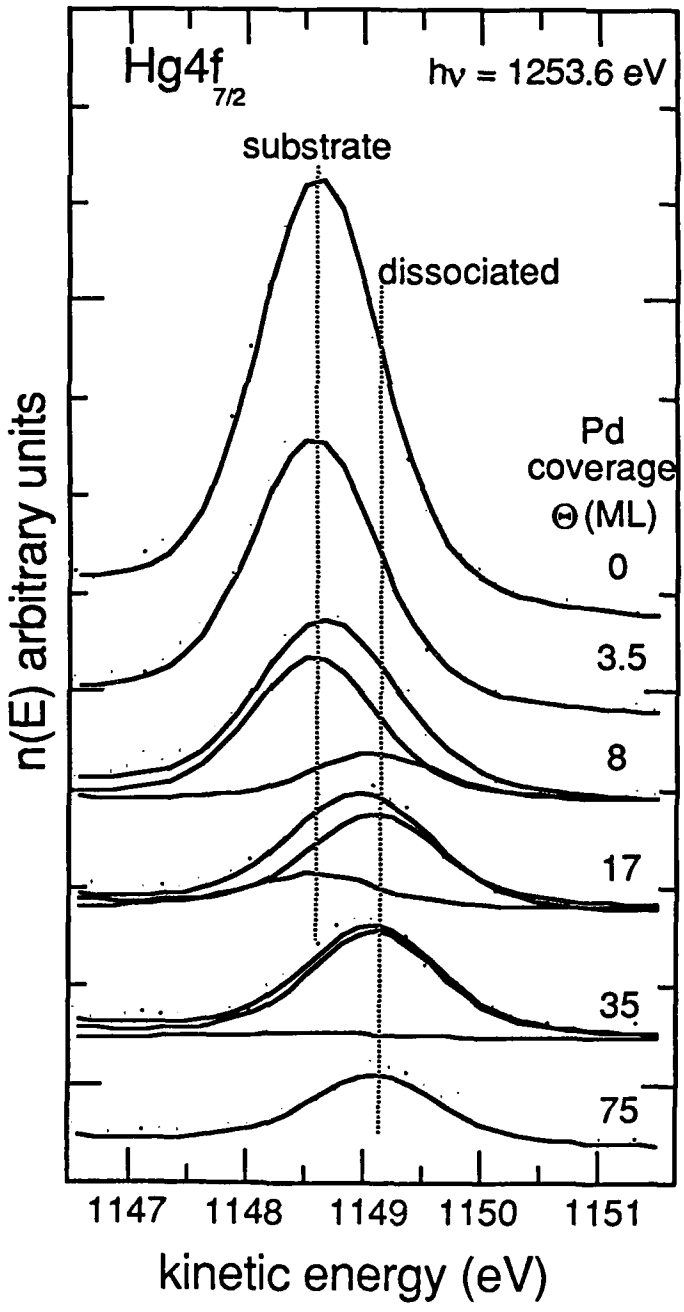

Figure. 4.11. PES spectra of the Hg $4f_{7/2}$ peak showing the results of the fit. The substrate and dissociated contributions are shown along with the raw data and the overall fit result. See the text for the details of the fit.

the fit) separately the cleaved spectra and the Hg feature at 75 ML, assuming one peak with a theoretical line shape given by a Lorentzian that is convolved with the Gaussian instrument broadening. After obtaining excellent fits to these endpoint spectra, the intermediate spectra were fit as linear combinations of these peaks. The results of the fit for the substrate and dissociated peaks are shown in Fig. 4.11 where the results for several coverages are shown. The raw data (data points) and total fit (substrate + dissociated) are shown along with the fitting results at each coverage. A separation of 0.5 eV is observed for the two Hg 4f features, which agrees favorably to the 0.4 eV shift to higher kinetic energy for the dissociated peak observed in the He I spectra of Fig. 4.8. Attempts to fit the dissociated Hg $4f_{7/2}$ contribution centered 0.4 eV to higher kinetic energy resulted in poor agreement with the data.

The resulting intensities of each Hg $4f_{7/2}$ peak are plotted in the top of Fig. 4.12, where it is seen that the attenuation of the substrate peak is roughly exponential. Both of the peaks are normalized to the initial intensity of the substrate peak. The expected attenuation, assuming an electron escape depth of roughly 15-20 Å, for an abrupt Pd overlayer is also shown in this figure. The actual attenuation of the substrate Hg signal is somewhat faster than for an ideal laminar Pd overlayer coverage, indicating that some substrate Hg is lost. As will be seen in the next two sections, the Cd and Te substrate components also attenuate faster than expected for an abrupt interface and laminar Pd overlayer growth.

B. Cd dissociation

Also shown in Fig. 4.8 are the Cd 4d core levels, where again at 8 ML coverage an appreciable contribution to the spectra arises from Cd that has a BE of approximately -10.25 eV. By the highest coverage of 75 ML, the sole Cd contribution to the spectra is

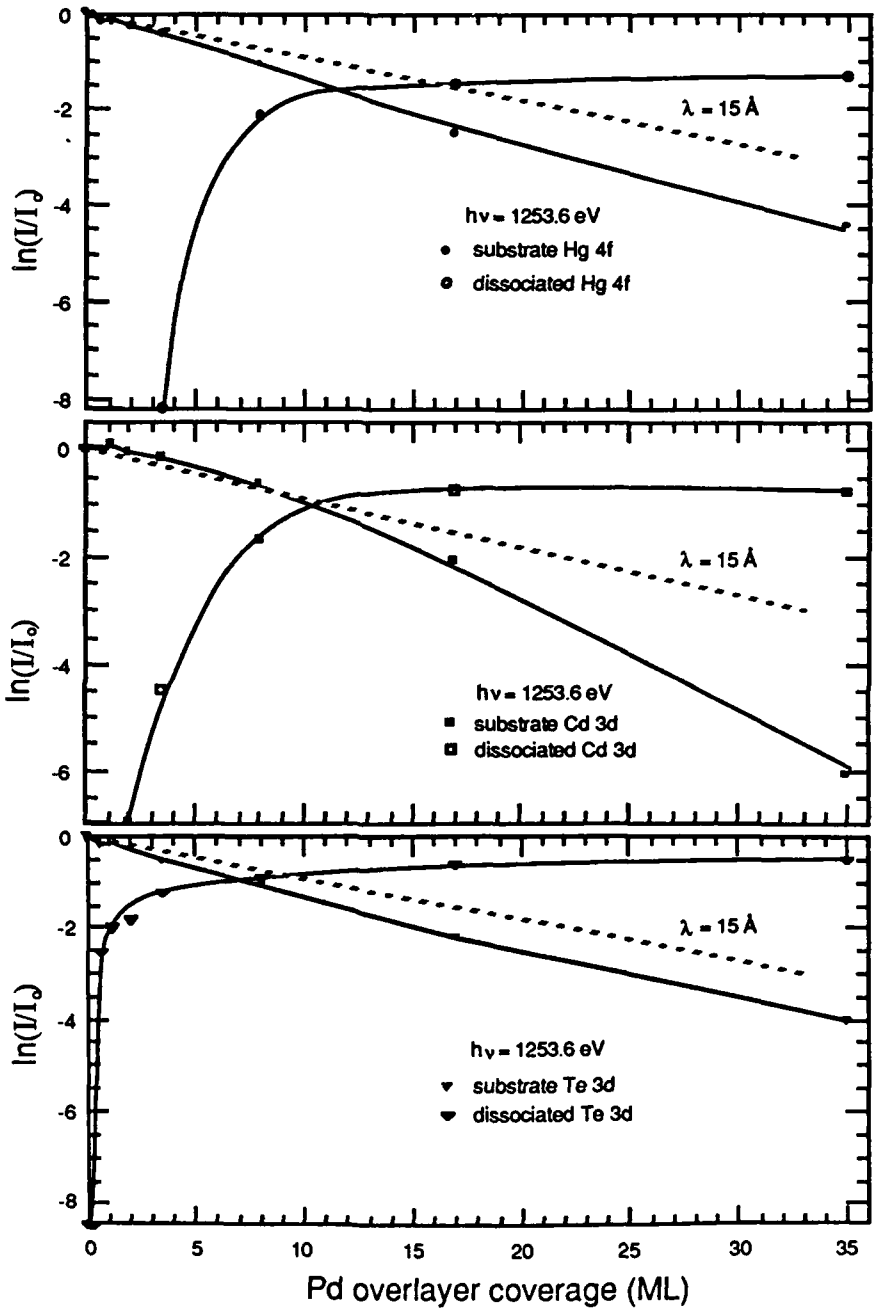

Figure. 4.12. Core level peak intensities versus Pd overlayer coverage. The top plot shows the results of the fit for the Hg $4f_{7/2}$ peak, the middle shows the resulting intensities of the Cd $3d_{3/2}$ features from the substrate and dissociated peaks, and the bottom shows the results for the Te $3d_{3/2}$ peaks. The dashed line in each plot shows the expected attenuation for an abrupt laminar overlayer.

centered at about -10.1 eV, which closely matches the BE expected for Cd that has dissociated from the substrate and alloyed into the Pd overlayer as outlined in the beginning of this section. Again, as with the Hg, there is a discernable contribution to the spectra at 75 ML, which indicates that the alloyed Cd is located in the near surface region. Referring again to Fig. 4.10, where the Cd signal is arising from the top 4 - 7Å, there is residual dissociated Cd signal at the highest coverages where little or no Hg intensity is observed. Thus there is dissociated Cd which is alloyed with the Pd that is located at the surface of the overlayer.

As mentioned in the previous section with the Hg 5d case, meaningful deconvolution of the substrate and dissociated Cd is not possible from the He spectra shown in Figs. 4.8 and 4.10 due to the overlap of the Hg $5d_{3/2}$ peak with the Cd 4d's. Deconvolution of both the substrate peak and the dissociated peak is possible by using the Cd $3d_{3/2}$ peak as shown in Fig. 4.13. The deconvolution was done in a similar manner as done for the Hg 4f case in Fig. 4.11. The best agreement of the fitting to the data was performed by free fitting the cleaved peak with one theoretical peak. The spectra at 35 ML coverage was then deconvoluted by fitting two peaks: the substrate contribution (fixing the energy centroid and width of the substrate peak, thereby only fitting the intensity) and a free fit of the dissociated peak. The resulting dissociated peak was employed along with the substrate peak as endpoint peaks to fit the intermediate coverage spectra. To fit to the intermediate coverage peaks, only the intensities of the two peaks were varied, thus forming linear combinations of the two. The two peaks are separated by 0.6 eV, with the dissociated peak centered at lower BE. The peak arising at 75 ML was fit assuming only one peak, but the centroid was shifted from the above dissociated peak position an additional 0.15 eV to higher kinetic energy. Attempts at using this 75 ML peak as an endpoint peak produced poor overall fits in the intermediate coverages. The shift to higher

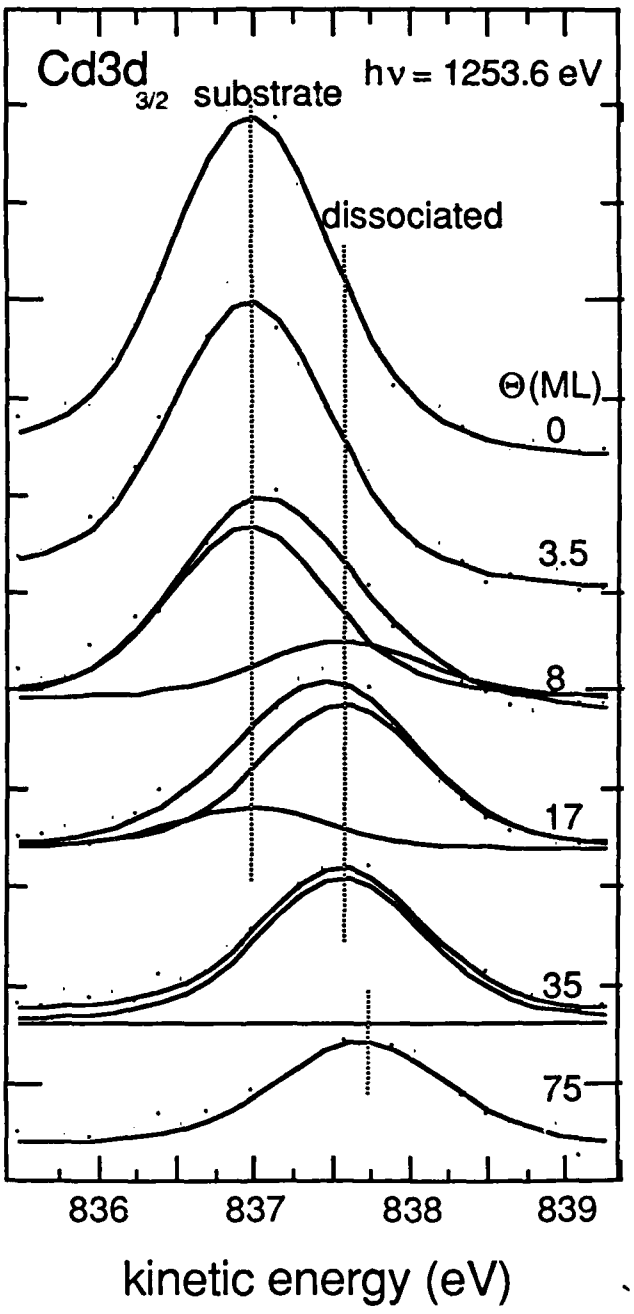

Figure. 4.13. PES spectra of the Cd $3d_{3/2}$ peak showing the results of the fit for several coverages of Pd. The substrate and dissociated contributions are shown along with the raw data and the overall fit result . See the text for the details of the fit.

kinetic energy observed in Fig. 4.13 for the highest coverage matches the shift observed in the He I spectra for the highest coverage. Both of the fitted peaks, along with the raw data and the overall fit are shown for several Pd coverages.

The resulting intensities of the Cd $3d_{3/2}$ substrate and dissociated peaks are shown in the middle of Fig. 4.12. The initial attenuation of the substrate peak follows very closely to that expected for an abrupt laminar overlayer, but at the higher coverages the intensity decreases more rapidly. Both of the peaks are normalized to the initial intensity of the substrate peak. The dissociated Cd peak rises in intensity until the 17 ML coverage, where little attenuation is observed for the 35 ML coverage. In going to the 75 ML coverage, which is not shown in this figure, it is evident from Fig. 4.13 that an appreciable signal from the dissociated peak persists.

C. Te dissociation

Figure 4.14 shows the total (substrate plus dissociated) peak areas of the Hg, Cd, and Te core levels as a function of Pd overlayer coverage, normalized to their initial intensity at the cleaved surface. Of the more bulk sensitive peaks (Hg 4f, Cd 3d, and Te 3d) shown in the figure, all show little attenuation at the lower coverages (< 5 ML), but for higher coverages the Te 3d signal decreases the slowest. Also shown are the more surface sensitive peaks arising from the Hg 5d and Cd 4d, where the increase in overall Cd signal is evident for coverages less than 15 ML. The Te 3d signal persists at the higher coverages, indicating that Te might be coming to the surface. Direct evidence of Te dissociation is given by examining Fig. 4.15, where the Te $3d_{3/2}$ peak is plotted for several Pd coverages. A contribution to the spectra at lower kinetic energy forms by the 3.5 ML coverage, and increases in intensity until the 75 ML coverage. The shift of this peak ~ 0.8

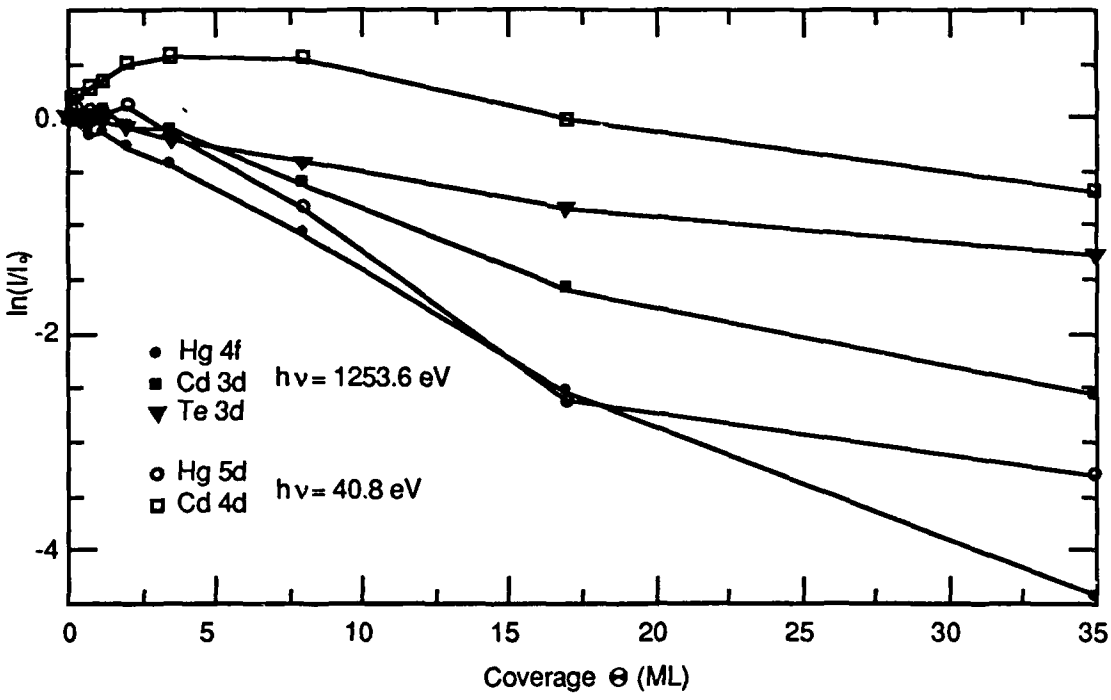

Figure. 4.14. PES spectra of the total (substrate + dissociated) intensity of the semiconductor core peaks. The Hg 5d and Cd 4d taken with He II are more surface sensitive than the spectra taken with hν = 1253.6. The Te 3d intensity falls the slowest at the higher coverages.

eV to deeper BE matches closely to that of elemental Te as reported in Ref. [32], where a shift of 0.7 eV was attributed to elemental Te.

Following the procedure outlined above, the substrate and dissociated peaks were fit by assuming the cleaved peak and the 75 ML coverage peak to be the endpoint peaks. The intermediate peaks were fit as linear combinations of the these two peaks, and the results are shown in Fig. 4.15. The intensities of these peaks versus Pd coverage are shown in the bottom part of Fig. 4.12, where the intensities are normalized to the zero-coverage value of the substrate Te 3d peak. In contrast to the Hg and Cd fitting results

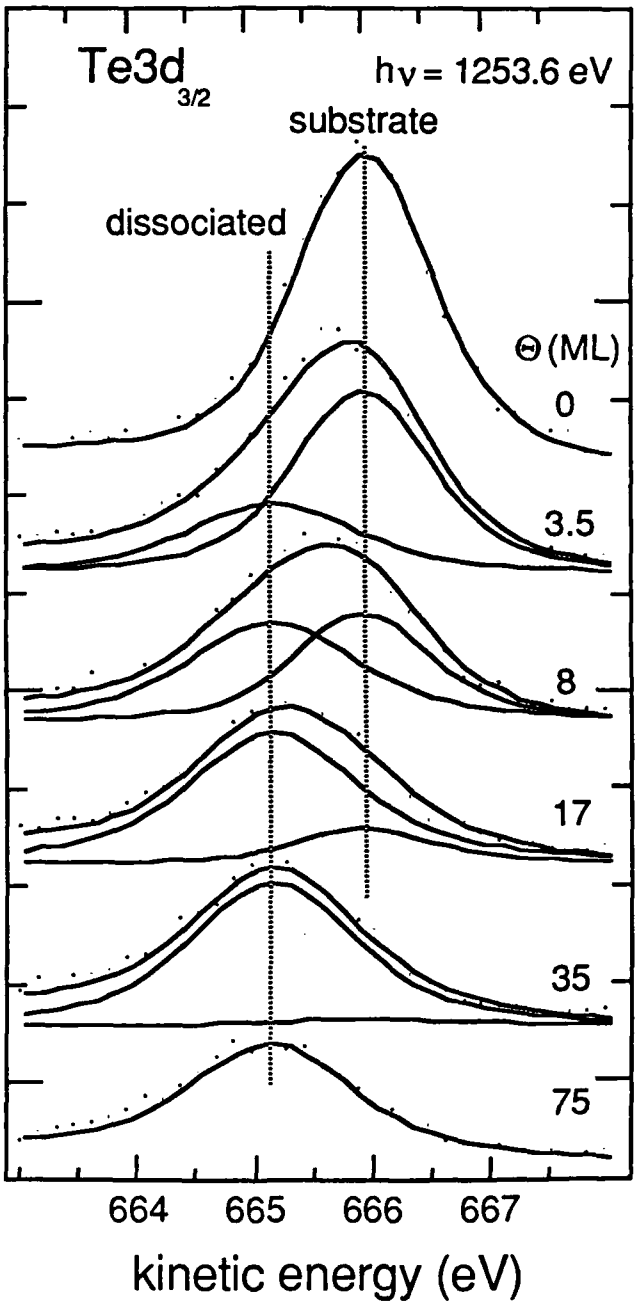

Figure. 4.15. PES spectra of the Te $3d_{3/2}$ peak showing the results of the fit for several coverages of Pd. The substrate and dissociated contributions are shown along with the raw data and the overall fit result . See the text for the details of the fit.

shown in Fig. 4.12, the Te dissociated signal increases rapidly at about 1 ML Pd coverage, whereas the Hg and Cd dissociated peaks give rise to an appreciable signal only after the 3.5 ML coverage. The dissociated Te reaches a higher intensity relative to the initial substrate intensity than is seen for the Hg and Cd dissociated peaks, and even at the highest coverage studied, 175 ML Pd, there is still discernable dissociated Te signal, whereas no Cd or Hg is seen at this highest coverage. The persistence of the Te dissociated signal even at 175 ML Pd coverage suggests that the dissociated Te is coming to the surface. Elemental Te has been observed to float on the surface of the Pt/HgCdTe interface [25], where there was evidence for a Te layer 7-8 Å thick on top of the Pt overlayer.

Additional information into the nature of the Te interaction with the overlayer is provided by examining the Pd 3d BE versus overlayer coverage. Fig. 4.16 gives the BE shift of the Pd 3d core level as a function of coverage. As more Pd is deposited on the surface, the BE decreases. This decrease is most rapid for coverages less than 8 ML. The value reached at the highest coverage is within ± 0.1 eV of the BE for metallic Pd given by Ref. [30]. The BE of the initial Pd peak is 1.1 eV deeper than the final metallic value. This could be due to absorbed unreacted atomic Pd on the surface, or small Pd clusters forming at the lower coverages. Fig. 4.9 shows that there is emission from the E_f at 0.7 ML, and the E_f is fully established by 3.5 ML Pd coverage. It is not unusual for small metallic clusters to exhibit deeper BE shifts, and Wertheim [33] has measured a 1.3 eV shift in the Cd 3d core level to deeper BE for small coverages of Pd on amorphous carbon substrates. Further evidence that the Te is not intermixed into the Pd overlayer but is phase separated is given by the Pd 3d BE energy position at high coverages. If the Te was reacted with the Pd, the Pd 3d BE would be less than the metallic value, which is not observed.

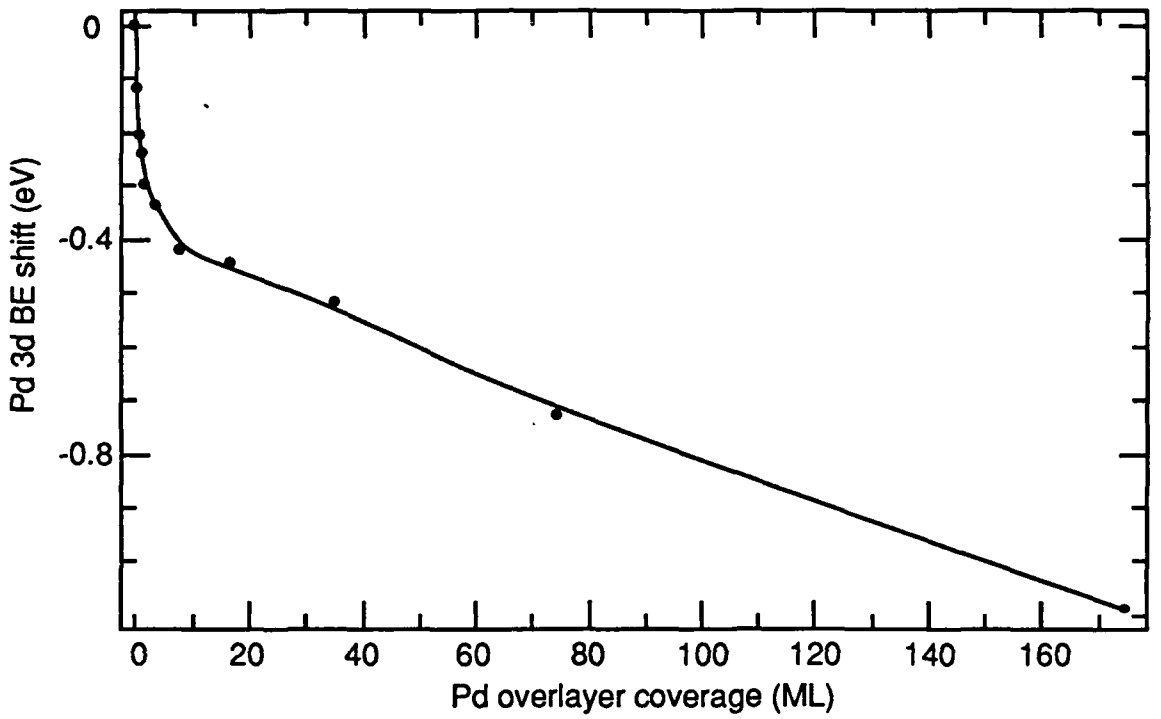

Figure. 4.16. The binding energy shift of the Pd $3d_{5/2}$ peak as a function of Pd deposition. After the rapid decrease in the lower coverages, the BE falls to the value of metallic Pd at the highest coverage. The spectra were taken with hν = 1253.6.

D. LEED observations

The data presented thus far indicate that the interface between Pd and HgCdTe is non-abrupt, with all of the semiconductor substrate constituents dissociating from the HgCdTe lattice and mixing into the overlayer with Te coming to the surface. Obviously, the concept of interface becomes difficult to define when all of the constituents are intermixing and the substrate is being consumed during the overlayer formation. The complexity of this interface is underlined by the observations from the LEED patterns that were taken subsequent to each deposition. For this RT formed Pd/HgCdTe interface, there

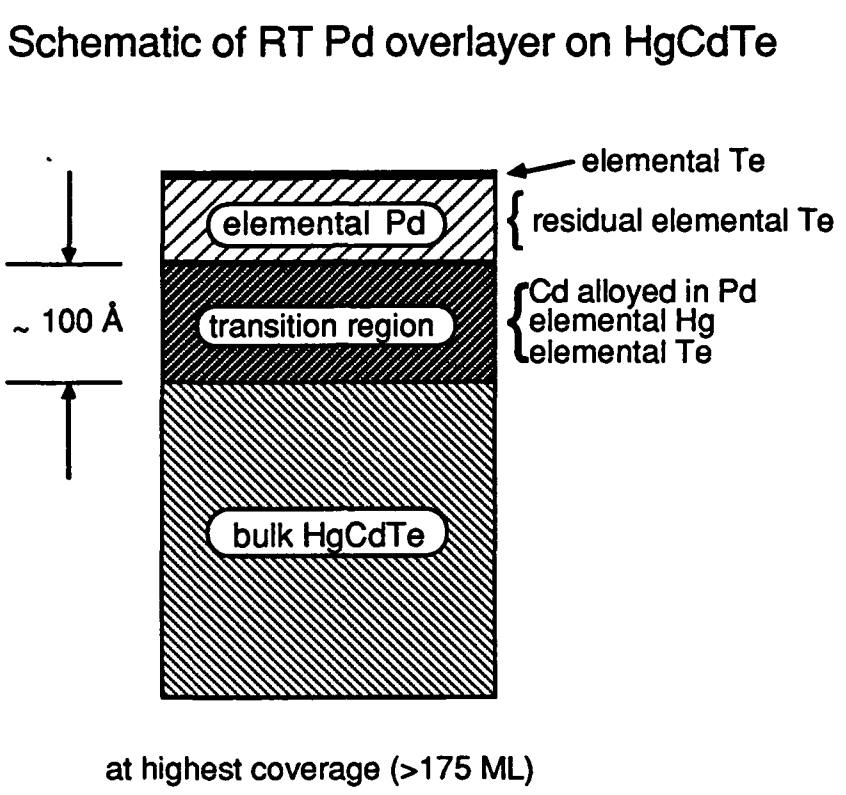

Figure. 4.17. Schematic drawing of the morphology of the Pd/HgCdTe interface at the highest coverage studied (175 ML). The interface is very disrupted, with the substrate constituents all dissociating and moving into the Pd overlayer.

is still a discernable LEED pattern at 8 ML coverage. Hence, there are still crystalline areas on the order of the coherence length of LEED (50 - 500 Å) exposed on the surface after this coverage of Pd.

This can be understood as either the Pd overlayer islanding on the HgCdTe surface, or that the Pd overlayer is growing epitaxially at the lower coverages. The fastest attenuation of the substrate core levels occurs upon formation of an abrupt interface with a 2-dimensional growth of the overlayer. Any islanding or clustering of the overlayer metal will cause the substrate core levels to attenuate more slowly than that expected for the ideal

abrupt interface (shown in Fig. 4.12 as the dashed lines, assuming an electron escape depth of 15 - 20 Å). As Fig. 4.12 reveals, all of substrate cores attenuate at the same rate or faster than for an abrupt interface. Hence, if the Pd is not covering the surface uniformly at the lowest coverages as the LEED pattern suggests, then epitaxial growth of the overlayer cannot be ruled out as a candidate mechanism of the growth of this interface. The rapid dissociation of the substrate during the formation of the Pd overlayer could result in the rapid attenuations observed for each of the substrate semiconductor peaks, but therefore it is difficult to obtain a clear picture of the exact mechanism of growth. Nevertheless, the interface is highly disrupted upon formation of the Pd overlayer. Fig. 4.17 shows schematically the interface at the highest coverages studied here. The Pd overlayer contains phase separated Te, with some Te likely at the surface, and a transition region on the order of 100 Å thick characterized by Cd alloyed into the Pd, elemental Hg, and some elemental Te.

IV. Growth of Pd on CdTe

A. Overview

The previous section presented experimental observations into the complexity of the Pd/HgCdTe interface formed at RT. This section presents data taken during the initial stages of formation of the RT grown interface between Pd and CdTe. Although there is no Hg present in the lattice, therefore no weak Hg-Te bond to increase the vulnerability of the lattice to disruption upon overlayer formation, the RT formed interfaces of Pd/$Hg_{0.61}Cd_{0.39}Te$ and Pd/CdTe are quite similar. The reaction with the substrate causing dissociation of both the Cd and the Te from the semiconductor occurs, but the extent of the disruption is less. There is also appreciable band bending at the initial Pd coverage, which is expected for *n*-type CdTe [34 - 36], the doping type of the crystal used in this study.

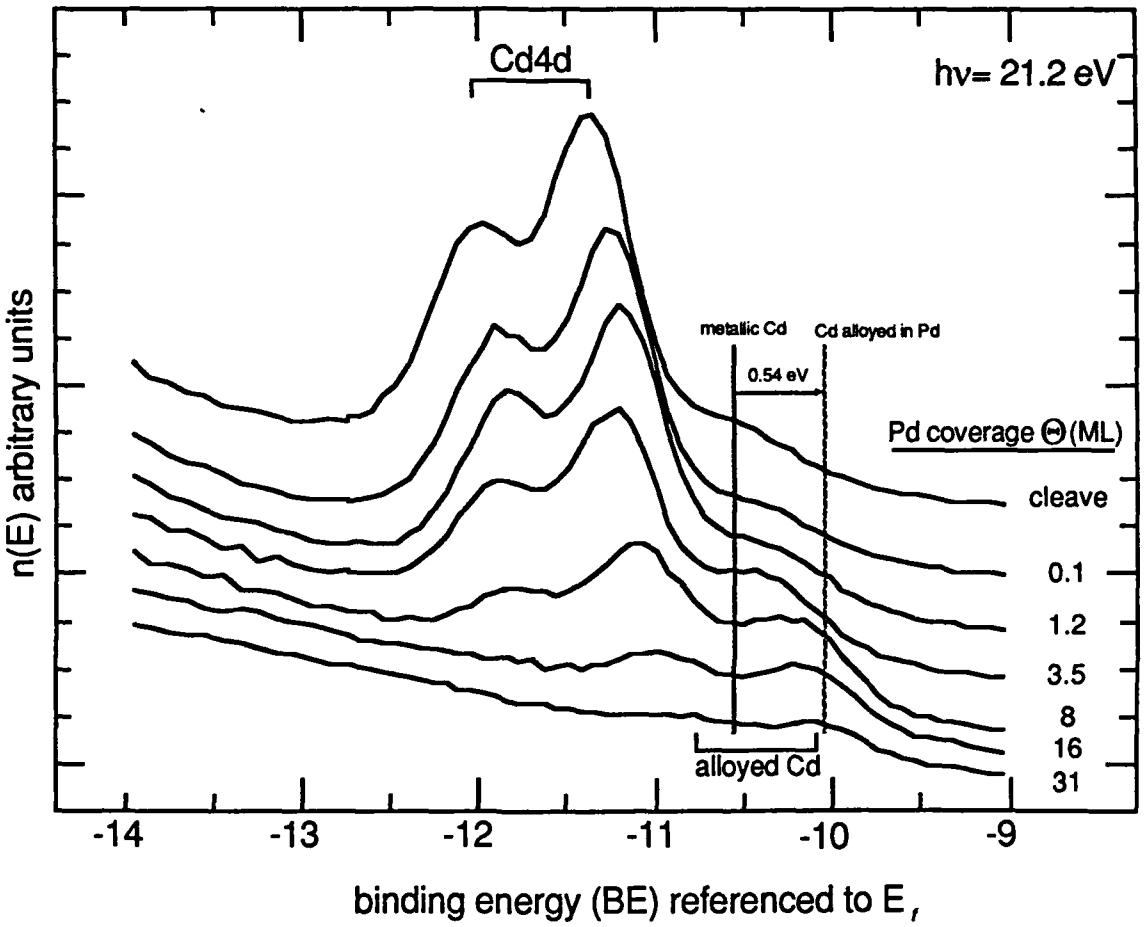

Figure. 4.18. He I spectra of the shallow Cd 4d core level versus Pd overlayer coverage. After an initial shift of 0.15 eV attributed to band bending at the lowest coverage, a new spectral feature arises at lower BE for the higher coverages which is attributed to Cd alloyed into the Pd overlayer.

B. Pd/CdTe results

i. *Cd dissociation*

Direct evidence for Cd dissociation is given in Fig. 4.18, where spectra taken with He I excitation are shown as a function of Pd overlayer coverage. The Cd 4d shallow core level shifts 0.15 eV to lower BE at the initial coverage. Since all of the spectra features

move together at this initial coverage, this shift is attributed to band bending. At 1.2 ML Pd coverage, a new peak begins to form at lower BE, and increases in intensity until it dominates the shallow core emission at 16 ML. As in the He I spectra shown in Fig. 4.8, this spectral feature is attributed to be from Cd that has dissociated from the CdTe substrate and moved into the Pd overlayer and alloyed with the Pd. As the coverage increases, the centroid of this peak moves to lower BE, approaching the position expected for Cd alloyed in Pd in infinite dilution, as discussed in association with Table 4.1. The BE of the Cd $4d_{5/2}$ peak at the cleaved surface is -11.35 eV, placing the E_f 1.05 above the VBM at the cleave. The peak moves to -11.20 eV at low coverages, and remains at this position for the higher coverages. Hence, the E_f pins at 0.90 eV above the VBM which is a typical value observed at metal/CdTe interfaces.

Because of the overlap in valence spectral features for the Cd 4d's in the He I spectra, it is difficult to accomplish meaningful deconvolution of the substrate and dissociated peaks for the curves shown in Fig. 4.18. The Cd $3d_{3/2}$ once again can provide for meaningful separation of the substrate and dissociated peaks as outline in the previous section for Fig. 4.13. This is shown for the CdTe case in the left side of Fig. 4.19, where the substrate, dissociated, and overall fit curves are plotted along with the raw data for several coverages of overlayer Pd. After free fitting the substrate spectra and shifting the centroid to accommodate band bending, the dissociated peak was determined by fixing the width and centroid of the substrate peak and free fitting the dissociated Cd peak at the 31 ML coverage. The intermediate spectra were fit with linear combinations of these and the results are shown in the figure. The separation of 1.0 eV between the two peaks, with the dissociated peak located to higher kinetic energy than the substrate peak, compares well with that observed in Fig. 4.18, where a 1.0 eV separation is also observed. The intensities of these peaks are plotted as a function of Pd coverage in the top of Fig. 4.20,

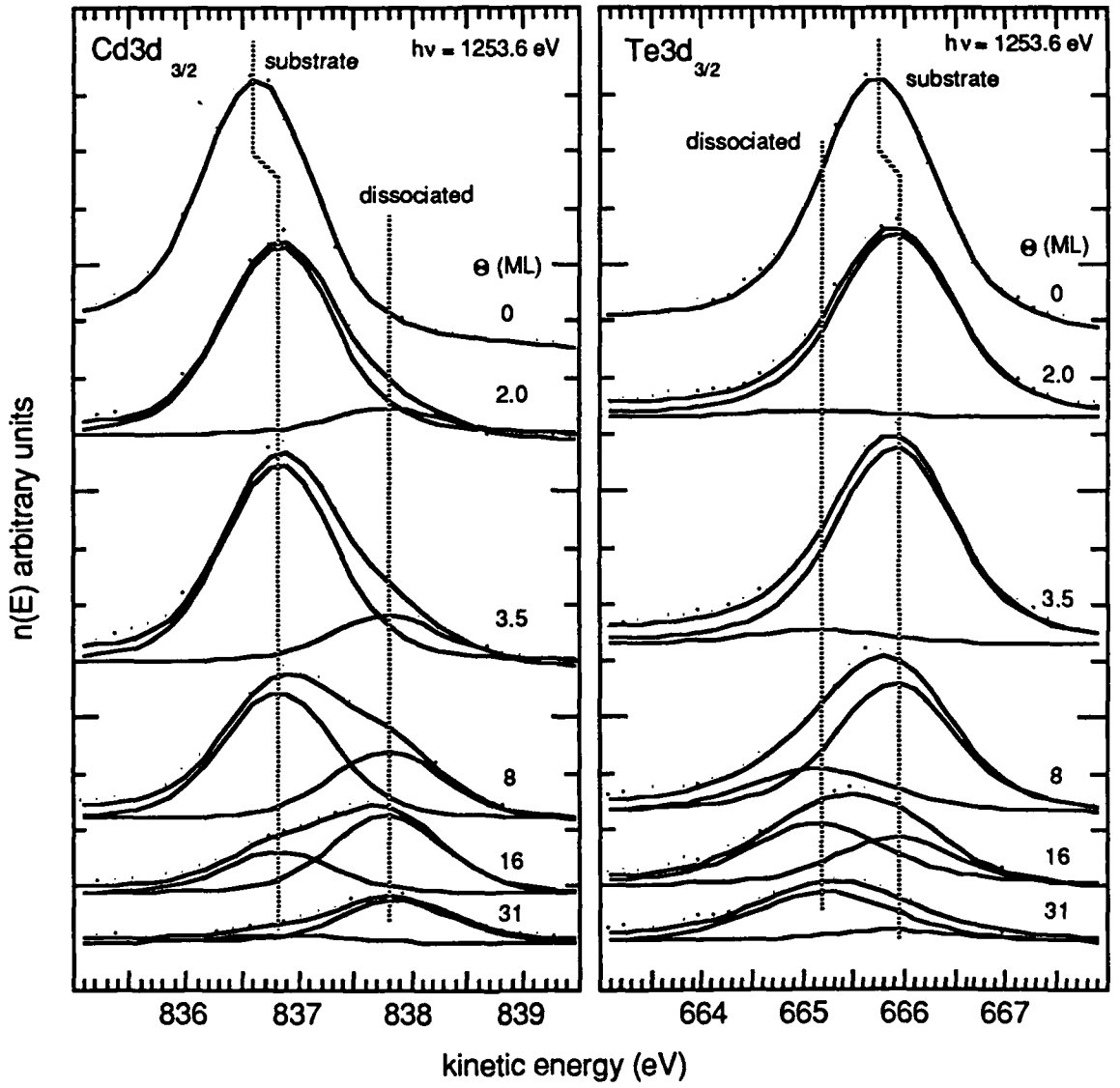

Figure. 4.19. PES spectra of the Cd $3d_{3/2}$ (right side) and Te $3d_{3/2}$ (left side) peaks showing the results of the fits for several coverages of Pd. The substrate and dissociated contributions are shown along with the raw data and the overall fit result. See the text for the details of the fit.

where the peaks have been normalized to the initial intensity value of the substrate peak. The attenuation of the substrate peak is once again close to that expected for a laminar overlayer coverage forming an abrupt overlayer. The maximum intensity for the dissociated Cd peak as a percentage of the initial Cd substrate intensity is less than that observed for the Cd at the Pd/HgCdTe case shown in Fig. 4.12. The decrease in the percentage Cd dissociated peak for the CdTe case indicates that less Cd has dissociated during the formation of this interface.

Additional information with regard to the uniformity of the overlayer is given by the Cd 4d spectra taken shown in Fig. 4.18. By 31 ML coverage, very little substrate Cd signal is seen. For the Cd 4d taken with He II, hence more surface sensitive, there is no substrate Cd signal from the interface, revealing that the overlayer has covered the substrate by this coverage. As will be discussed below, this result renders the LEED observations for this interface quite surprising and difficult to understand.

ii. *Te dissociation*

The right side of Fig. 4.19 shows the deconvolution of the substrate and dissociated Te $3d_{3/2}$ peaks for several Pd coverages. The peaks were fit as described for the Cd case above. The dissociated peak is located 0.9 eV to lower kinetic energy, which is attributed to elemental Te. The intensities of the two peaks as a function of Pd overlayer coverage are shown in the bottom of Fig. 4.20, where the peaks are normalized to the zero-coverage value of the Te $3d_{3/2}$ core level substrate intensity. The attenuation of the substrate peak matches very closely to what would be observed for electrons travelling through an abrupt laminar overlayer with an escape depth of 15 Å. The maximum dissociated Te signal as a percentage of the initial substrate intensity is much less than that observed at the Pd/HgCdTe interface shown in Fig. 4.12. This is indicative of the reduced

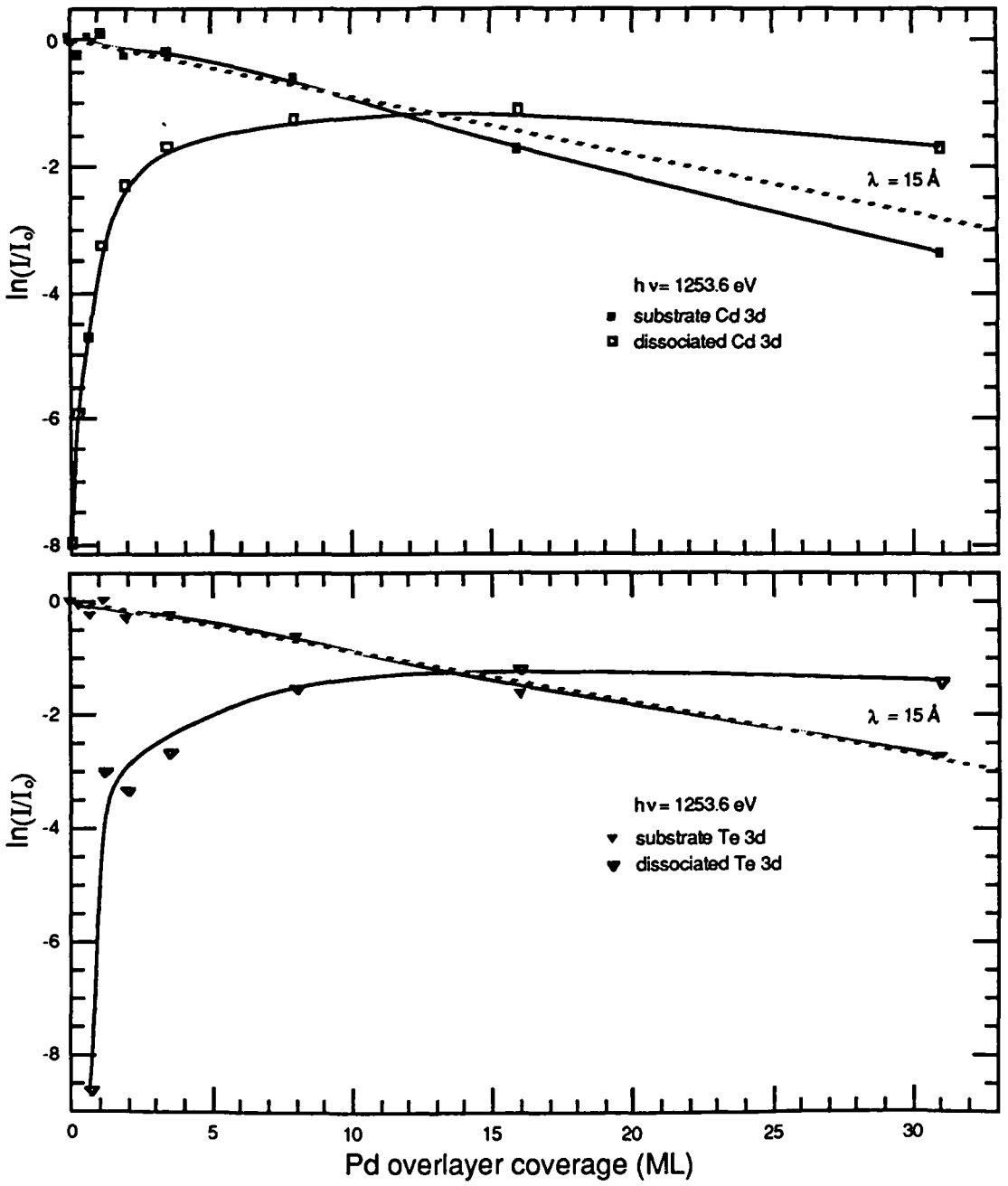

Figure. 4.20. Core level peak intensities versus Pd overlayer coverage. The top plot shows the results of the fit for the Cd $3d_{3/2}$ substrate and dissociated peaks, and the bottom shows the results for the Te $3d_{3/2}$ peaks. The dashed line in each plot shows the expected attenuation for an abrupt laminar overlayer.

disruption at this Pd/CdTe interface as opposed to the Pd/HgCdTe case. Less elemental Te is released into the overlayer due to lesser consumption of the substrate during the initial Pd coverages.

iii. *LEED observations*

LEED was performed subsequent to each deposition after the PES spectra were acquired. The surprising result of the observations of the LEED pattern is that there is still a discernable LEED pattern (although the spots are very faint) at 31 ML Pd overlayer coverage. Remember that there was still a LEED pattern at 8 ML Pd coverage for the HgCdTe case which is quite unexpected, but the LEED observations at this interface are difficult to understand. The data is highly suggestive of a registry of the overlayer to the substrate. Since the symmetry and the *d*-spacing of the pattern do not change but only become more faint with coverage, the registry would have to be epitaxial. Even limited epitaxial growth would be quite unexpected for UHV grown reactive overlayers on semiconductor surfaces. No such similar behavior was observed at the Pt/HgCdTe interfaced [25] where the LEED pattern had disappeared by 0.6 ML, but the existence of a LEED pattern at 10 ML coverage has been observed for the Pt/CdTe interface [37].

V. Summary of RT Pd interfaces formed on HgCdTe and CdTe

As shown the previous two sections, the RT interfaces formed between Pd and HgCdTe and CdTe are quite complex chemically and morphologically. Dissociation of both the substrate cations and anions are observed at each interface. The Cd moves into the overlayer and alloys with the Pd, whereas there is spectroscopic evidence that the Hg moves into the overlayer and exists in its elemental form. The Te does not react with the Pd, but rather moves toward the surface and remains phase segregated as elemental Te. Little band bending is observed at the RT Pd/HgCdTe interface, and a shift of 0.15 eV

from the cleave position of 1.05 eV above the VBM to a pinning position of 0.90 eV above the VBM is seen at the RT Pd/CdTe interface. The rapid attenuation of all of the substrate core levels suggests that there is uniform growth of the overlayer, but the LEED results suggest that there are still areas on the surface that have not been covered. Consistent with both of these observations is that the overlayer that forms on the surface does so epitaxially at the lower coverages. Yet most of the chemistry and intermixing occurs between the overlayer and the substrate at these lower coverages, which should "tear up" the surface. Speculation aside, the main conclusions that can be drawn from this study of the RT temperature interfaces formed between Pd and HgCdTe and CdTe are that the semiconductor lattice is highly disrupted at the interface with a large intermixing of the substrate constituents into the reactive Pd overlayer.

Aknowlegdment

*Work supported by DARPA under contract # N00014-86-K0854.